Study of the Valence Wave Function of Thiophene with High Resolution Electron Momentum Spectroscopy and Advanced Dyson Orbital Theories

Y. R. Huang,[†,‡] B. Hajgató,[‡] C. G. Ning,[†] S. F. Zhang,[†] K. Liu,[†] Z. H. Luo,[†] J. K. Deng,*[,†] and M. S. Deleuze*[,‡]

Department of Physics and Key Laboratory of Atomic and Molecular NanoSciences of MOE, Tsinghua University, Beijing 100084, P. R. China, and Research Group of Theoretical Chemistry, Department SBG, Hasselt University, Agoralaan, Gebouw D, B-3590 Diepenbeek, Belgium

Received: November 13, 2007; In Final Form: December 11, 2007

Results of an exhaustive experimental study of the valence electronic structure of thiophene using high resolution electron momentum spectroscopy at impact energies of 1200 and 2400 eV are presented. The measurements were performed using an electron momentum spectrometer of the third generation at Tsinghua University, which enables energy, polar and azimuthal angular resolutions of the order of $\Delta E = 0.8$ eV, $\Delta\theta = \pm 0.53°$ and $\Delta\phi = \pm 0.84°$. These measurements were interpreted by comparison with Green's function calculations of one-electron and shake-up ionization energies as well as of the related Dyson orbital electron momentum distributions, using the so-called third-order algebraic diagrammatic construction scheme (ADC(3)). Comparison of spherically averaged theoretical electron momentum distributions with experimental results very convincingly confirms the presence of two rather intense $\pi^{-2}\,\pi^{*+1}$ shake-up lines at electron binding energies of 13.8 and 15.5 eV, with pole strengths equal to 0.18 and 0.13, respectively. Analysis of the electron momentum distributions associated with the two lowest $^2A_2$ (π_3^{-1}) and $^2B_1$ (π_2^{-1}) cationic states provides indirect evidence for a symmetry lowering and nuclear dynamical effects due to vibronic coupling interactions between these two states. ADC(3) Dyson orbital momentum distributions are systematically compared with distributions derived from Kohn−Sham (B3LYP) orbitals, and found to provide most generally superior insights into experiment.

I. Introduction

Electron momentum spectroscopy (EMS) is a highly efficient experimental tool for studying the electronic structure of atoms, molecules and solids.[1−3] This technique is based on kinematically complete (e, 2e) electron impact ionization experiments ($M + e^- \rightarrow M^+ + 2e^-$), which, from an analysis of the angular dependence of ionization cross sections, enable an experimental reconstruction of electron momentum densities associated with individual ionization channels, i.e., of orbital densities in a simple one-electron picture of ionization. Phase relationships are also amenable through the analysis, which most often enables a rather straightforward and unambiguous characterization of the topologies and symmetry characteristics of the ionized orbitals. Therefore, although orbitals are not true quantum observables, EMS is most commonly regarded as a powerful "orbital imaging" technique. With EMS, the whole valence energy region is accessible with an energy resolution that is comparable with that reached in X-ray photoelectron spectroscopy (typically, from 0.5 to 1.0 eV). In practice, the ionization spectrum is measured by collecting in coincidence the two outgoing electrons at fixed energies and as a function of the azimuthal angle ϕ under which these electrons are ejected, whereas the energy of the impinging electron is smoothly varied. As with any ionization experiment, the position of a band in the electron binding energy spectrum is determined by the energy difference between the initial (neutral) state $|\Psi_0^N\rangle$ and the final (cationic) state $|\Psi_n^{N-1}\rangle$ in the ionization process, whereas the associated intensity is a function of the partial overlap between these two states, defining a Dyson orbital[4]

$$g_n(\mathbf{x}) = \sqrt{N} \int \Psi_n^{N-1}(\mathbf{x}_1,\mathbf{x}_2,\cdots,\mathbf{x}_{N-1}) \Psi_0^N(\mathbf{x}_1,\mathbf{x}_2,\cdots,\mathbf{x}_{N-1},\mathbf{x})\, d\mathbf{x}_1\, d\mathbf{x}_2 \cdots d\mathbf{x}_{N-1} \quad (1)$$

with N the number of electrons, and where $\mathbf{x}$ denote spin-space coordinates $\mathbf{x} = (\omega, \vec{r})$.

In EMS, (e, 2e) ionization intensities at high electron impact energies are simply proportional to electronic structure factors obtained as the squares of the Fourier transforms of Dyson orbitals. In an exact theory of ionization, Dyson orbitals are introduced as effective orbitals for the ionized electrons, which account for both ground state correlation and dynamical relaxation effects, as well as for the dispersion of the ionization intensity over states relating to excited (shake-up) states of the cation. Their norms are equal to spectroscopic pole strengths (Γ_n) measuring the probability that the removal of one electron from an occupied orbital in the molecular target will lead to a specific ionic state $|\Psi_n^{N-1}\rangle$. When electron correlation and relaxation effects are neglected (Koopmans's approximation), Dyson orbitals reduce simply to Hartree−Fock (HF) orbitals, the corresponding ionization energies simplify to minus the relevant HF orbital energies, and the associated pole strengths become equal to one.

In practice, Dyson orbitals are very hard to compute and have most commonly been empirically approximated by Kohn−Sham

* Corresponding authors. J.K.D. e-mail: djk-dmp@tsinghua.edu.cn. M.S.D. e-mail: michael.deleuze@uhasselt.be.
† Tsinghua University.
‡ Hasselt University.

10.1021/jp710845n CCC: $40.75
Published on Web 02/21/2008

(KS) orbitals that were obtained from calculations employing density functional theory (DFT) and standard functionals such as the BP86 (Becke−Perdew 1986)[5] or B3LYP (Becke-3-parameter−Lee−Yang−Parr)[6] functionals. Because of the neglect of many-body interactions, HF orbitals are not suited for a quantitative analysis of (e, 2e) electron momentum distributions. KS orbitals obtained from standard DFT calculations do account for the influence of electronic correlation on the ground state energy, but not for configuration interactions in the final cationic state. In addition, assuming an extension of Koopmans's theorem to DFT, the related orbital energies are known[7] to yield systematic and particularly severe underestimations, by a few eV, of the experimental ionization energies, due to an incomplete compensation to the self-interaction error and an incorrect decay[8] of the electronic potential in the asymptoptic region ($r \rightarrow \infty, p \rightarrow 0$) therefore. From a qualitative viewpoint, HF, KS and Dyson orbitals exhibit most usually very similar shapes, regardless of their spread which may significantly vary depending on the way electronic correlation is treated in the modeling. EMS enables therefore detailed experimental insights into the chemical bonding characteristics of molecules, as well as into the influence of the correlation of electronic motions on the electronic wave function itself. This is particularly true for the outer valence orbitals, which in turn govern most chemical properties, and above all, chemical reactivity.[9,10] Note nonetheless that, because of particularly large errors on ionization energies, it is not advisable *at all* to use only KS orbitals and their energies to interpret highly congested EMS ionization spectra.[11] Widespread applications of EMS[12] in studies of the outermost orbitals in various types of molecules have shown that the method is particularly sensitive indeed to those aspects of the electronic structure that are most important for determining chemical bonding characteristics such as π-, σ- or hyper- and through-space conjugations, anomeric interactions and lone-pair delocalizations as well as for unraveling the influence of the molecular architecture (configuration, conformation,[13] cyclic strains,[11,14] ...) on the electronic structure. Since the computed electron momentum distributions are rather sensitive to electronic correlation effects, it is also most tempting to use EMS as a tool for comparatively evaluating the quality of various wave functions for neutral ground states, prior to computing further molecular properties. There is indeed most often a reasonably good correlation between the quality of the computed electron momentum distributions and that of molecular properties,[14] such as infrared frequencies, NMR shifts or electric dipole moments. One should however always remember that EMS experiments are inherently subject to the many complications that most usually affect ionization experiments, such as distorted wave effects,[15] shake-up processes,[13b] or vibronic coupling interactions,[16] whereas other properties are also subject to complications of their own (for instance, anharmonic effects when considering vibrational spectra).[14b] In practice, extensive and accurate enough theoretical calculations are therefore required if the interpretation of EMS experiments is to have any quantitative value at all.

The compound of interest in the present work is the five-membered heterocyclic and aromatic thiophene compound (C_4H_4S). This molecule is essential for industrially important processes such as the synthesis of biologically active compounds, or the manufacture of pesticides and semiconducting organic polymers.[17,18] Thiophene molecules form the structural units of many natural products and are the building blocks for the making of promising novel materials[19] exhibiting a variety of intra- and intermolecular interactions (van der Waals interactions, hydrogen bonds, $\pi-\pi$ stacking and sulfur−sulfur interactions[20,21] ...). Thiophene-based materials are in particular very ideally suited for the making of organic thin film transistors.[22−24]

The outer valence shell photoelectron spectrum of thiophene has been studied extensively experimentally, using ultraviolet photoelectron spectroscopy (UPS) under He I[25,26] or He II radiation,[26] synchrotron radiation photoelectron spectroscopy (SRPES),[27−29] X-ray photoelectron spectroscopy (XPS),[30,31] Penning ionization electron spectroscopy (PIES),[25,32,33] and electron momentum spectroscopy (EMS).[34] The latter EMS study was carried out at Tsinghua University using an experimental setup from the second generation, thus major drawbacks in that work were the rather low statistical accuracy and the limited energy and angular resolution ($\Delta E = 1.0-1.2$ eV, $\Delta\theta = \pm 0.6°$ and $\Delta\phi = \pm 1.2°$). Another limitation in this first EMS work on thiophene stemmed from the one-electron picture of ionization that was used to interpret all valence bands in the (e, 2e) ionization spectra. In the present work, we report an exhaustive experimental EMS investigation, at higher resolutions and statistical accuracy than any study so far ($\Delta E = 0.8$ eV, $\Delta\theta = \pm 0.53°$ and $\Delta\phi = \pm 0.84°$),[35] of the momentum distributions associated with all valence orbitals of thiophene, throughout the valence region, up to electron binding energies of ~45 eV. The main scopes of the present work are to experimentally probe in more detail the molecular orbital characteristics throughout the valence region, and confirm from the measured electron distributions the presence in the valence bands of rather intense ionization lines related to electronically excited (shake-up) configurations of the cation.

It is indeed well-known that the energy released by electronic relaxation is most often largely sufficient to induce numerous electronic excitation processes within the cation, yielding a very significant dispersion of the ionization intensity over many shake-up states with individually low intensities. This is particularly true for large conjugated and/or aromatic systems.[36−40] With these systems the dispersion of the ionization intensity into many-body processes is such that for many ionization bands, in both the inner- and outer-valence region, it is strictly impossible to discriminate the shake-up states from the one-electron ionization lines to which they borrow their intensity. To accurately describe one-electron binding energies and properly account for these secondary structures in the ionization spectrum, one must resort to theoretical methods which deal with the effects of both electron correlation interaction and relaxation, taking into account the outcome of multiconfiguration interactions in the initial and final states.

Theoretical studies of the electronic structure of thiophene accounting for satellite structures in the ionization bands are comparatively scarce. These comprise the early Green's function treatment by G. Bieri et al.,[41] the calculations by D. M. P. Holland et al.[29] using one-particle Green's function (1p-GF) theory[42−45] along with the so-called third-order algebraic diagrammatic construction scheme [ADC(3)],[36,46−48] as well as recent large-scale calculations by M. Ehara et al.[49] employing a valence triple-ζ basis set augmented by polarized functions and the general-R extension of the symmetry-adapted-cluster configuration-interaction approach (abbreviated as SAC-CI general-R).[50] A further work of immediate relevance for the present study is a very thorough analysis by A. B. Trofimov et al.[51] of the very intricate vibrational structure of the two outermost valence bands in the He I photoelectron spectrum of thiophene by Derrick et al.,[52] using a linear vibronic coupling model in conjunction with calculations of vibrational frequencies and ionization energies at the level of the second-order Moller−

Plesset perturbation theory (MP2)[53] and the outer valence Green's function (OVGF) approach,[54] respectively.

In addition to very severe breakdowns of the one-electron (orbital) picture of ionization in the inner-valence region, leading to a dispersion of the ionization intensity over highly congested sets of shake-up lines of very limited intensities, all the above cited studies of the photoelectron spectrum of thiophene give theoretical evidence for a substantial contamination of both the outer-valence σ- and π-band systems by shake-up lines at extremely low ionization energies and with rather significant strength. Similar features have been observed previously in extensive 1p-GF studies of the ionization spectra of many large conjugated systems such as polyenes[55] and, in particular, 1,3-butadiene,[13b] carbon clusters,[36,38,39] benzene[40,47] and polycyclic aromatic hydrocarbons,[40,56] stilbene,[14b] furan and pyrrole,[29] purine and pyrimidine,[57] chlorobenzene[58] as well as a number of thiophene derivatives.[59−61]

Reminding that no theory so far ever formally proved that an analytical relationship prevails between KS orbitals derived for interacting many-electron systems from DFT calculations on neutral molecules and Dyson orbitals measuring partial overlaps between neutral and cationic wave functions, a further scope of the present work is to assess the quality of spherically averaged B3LYP electron momentum distributions through a confrontation with benchmark ADC(3) results. Such an assessment is motivated by the prevalence of Kohn−Sham momentum distributions in most theoretical works so far on EMS experiments.

II. Experimental Background

Electron momentum spectroscopy[1−3] is based on electron *impact* ionization experiments focusing on (e, 2e) reactions ($M + e^- \rightarrow M^+ + 2e^-$) at high kinetic energies ($E_0 \gg 1$ keV, with E_0 the energy of the impinging electron). An energy-dispersive multichannel electron momentum spectrometer with a symmetric non-coplanar scattering geometry[1−3] was used in the experiment described in this work. In such a geometry, the two outgoing electrons are selected at equal polar angles ($\theta_1 = \theta_2 = 45°$) relative to the direction of incident electron beam. The relative azimuthal angle ϕ is the difference between the two outgoing electrons. Scanning through a range of ϕ is equivalent to sampling different target electron momenta p as[3]

$$p = \left[(2p_1 \cos\theta - p_0)^2 + 4{p_1}^2 \sin^2\theta \sin^2\left(\frac{\phi}{2}\right)\right]^{1/2} \qquad (2)$$

where p_1 and p_0 are the momenta of the outgoing and incident electrons, respectively. If the incident electron energy is varied, an electron binding energy spectrum can be recorded at each azimuthal angle ϕ. Variation of ϕ at a given binding energy therefore yields an orbital electron momentum (density) distribution. In the present work, a new experimental EMS measurement on thiophene was carried out using a spectrometer of the third generation which has been recently constructed at Tsinghua University, and which features a high coincidental count rate.[62] To achieve high resolutions, both in energies and electron momenta, significant modifications were implemented on this spectrometer. Briefly, an electron gun equipped with an oxide cathode, which worked at a much lower temperature than the generic filament cathodes, was used to generate the electron beam with low energy spread and low divergence angle. The electron beam size was constrained to 0.3 mm in diameter by a molybdenum aperture and the pass energy was set to 50 eV for improving the momentum resolution and energy resolution. Since the oxide cathode is easily poisoned by active gas, an additional vacuum chamber was especially designed to mount the electron gun. This chamber is evacuated to a base pressure of 10^{-7} Pa by a 600 L/s molecular turbopump, with a hole of 2 mm in diameter which connects to the main chamber in order to let the electron beam passing through. Thanks to these experimental parameters and an optimization of the electron optics using Monte Carlo simulations, the angle resolutions which could be achieved are $\Delta\phi = \pm 0.84°$ and $\Delta\theta = \pm 0.53°$, according to a standard calibration run for argon. The achieved momentum resolution is $\Delta p \sim 0.16$ au (fwhm) or $\Delta p = 0.069$ au (one standard deviation) at an impact energy (E_0) of 1200 eV. At $E_0 = 2400$ eV, Δp deteriorates slightly to 0.23 au (fwhm) or $\Delta p = \pm 0.098$ au (one standard deviation). The energy resolution is highly dependent on the emitting current of the cathode due to the space charge effects. The energy resolution $\Delta E = 0.45$ eV (fwhm) is obtained with an emitting current of 1 μA at an impact energy 1200 eV. This resolution deteriorates to $\Delta E = 0.8$ eV (fwhm) with around an emitting current of 10.0 μA.

III. Computational Details

Recent studies of the EMS spectra and momentum distributions (MDs) of 1,3-butadiene,[13b] dimethoxymethane,[12d] difluoromethane (CH_2F_2)[63] and water[35] have demonstrated that large-scale 1p-GF calculations employing the ADC(3) scheme enable not only quantitative calculations of the related ionization spectra but also straightforwardly accurate computations of Dyson orbitals in momentum space. It is worth noticing that most theoretical works on EMS experiments so far are based on the empirical assumption that normalized Dyson orbitals can be approximated by Kohn−Sham (KS) orbitals.[64,65] There is however no formal exact relationship between Kohn−Sham orbitals and Dyson orbitals as DFT calculations on neutral systems are not suited for describing shake-up states and configuration interactions in the cation.[13b] Note also that density functional theory (DFT) suffers from a number of severe fundamental limitations, like the neglect of electronic relaxation effects and, for most currently used exchange-correlation functionals, an incorrect behavior[8] of the electronic potential in the asymptotic region ($r \rightarrow \infty$, $p \rightarrow 0$). As a result, systematic underestimations of ionization energies by several eVs are systematically encountered.[14a]

The geometry of thiophene has been optimized using the aug-cc-pVTZ basis set[66] and density functional theory (DFT) in conjunction with the Becke−three-parameter-Lee−Yang−Parr (B3LYP) functional.[6] This approach is known to provide equilibrium geometries and related properties of quality comparable to that achieved at the benchmark CCSD(T) theoretical level.[67] All DFT, OVGF, and CCSD(T) calculations discussed in the present work have been performed using GAUSSIAN03.[68] The ADC(3) calculations have been carried out using the original 1p-GF/ADC(3) package of programs, interfaced to GAMESS.[69] This package incorporates a band-Lanczos[70] "pre"-diagonalization of the block matrices pertaining to the 2p-1h shake-on states into a pseudo-electron attachment spectrum, prior to a complete block-Davidson diagonalization[71] of the so-reduced ADC(3) secular matrix. With this diagonalization procedure, all eigenvalues of the ADC(3) secular matrix with pole strengths equal to (or larger than) 0.005 could be recovered up to electron binding energies of ~32 eV. The assumption of frozen core electrons has been used throughout, and the full molecular symmetry point group has been exploited. At the self-consistent field level, the requested convergence on each of the elements of the density matrix was fixed to 10^{-10}. The 1p-GF/

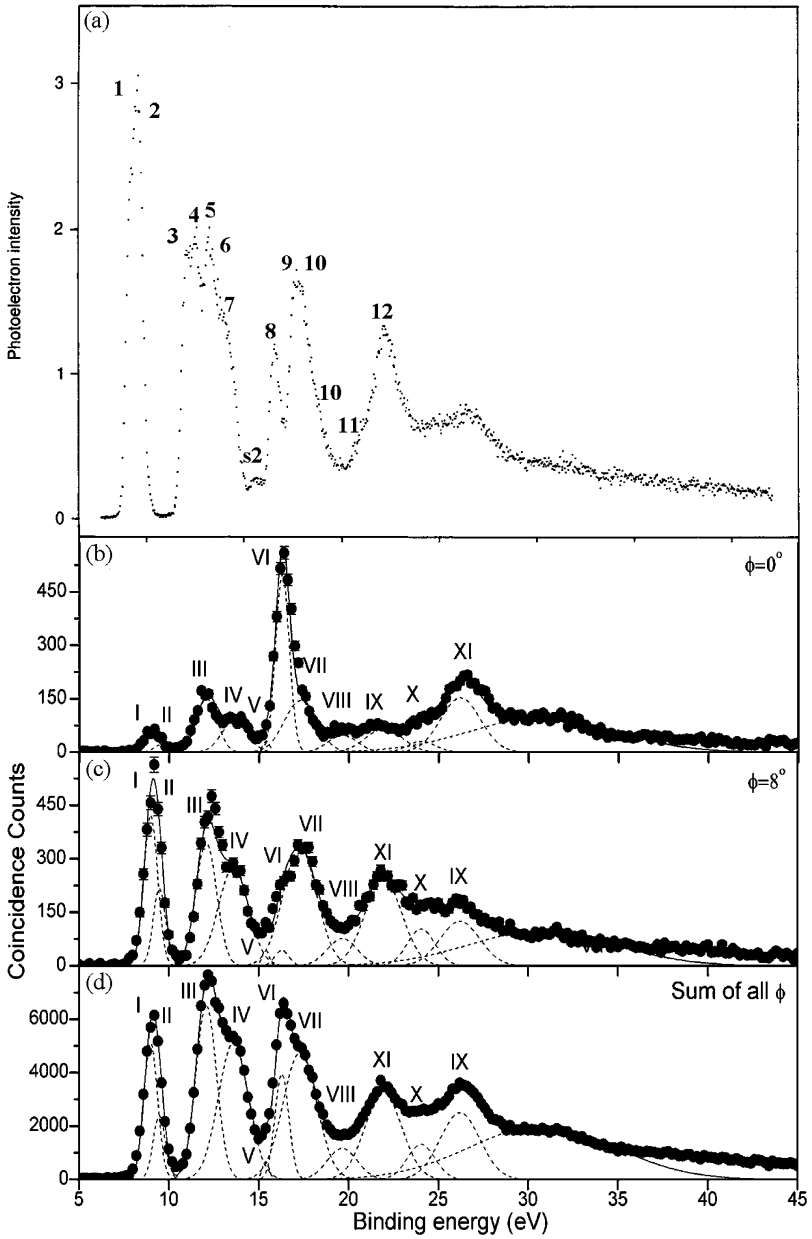

Figure 1. (a) The valence shell photoelectron spectrum of thiophene recorded at a photon energy of 90 eV.[29] (b) The valence shell EMS ionization spectra of thiophene at azimuthal angle $\phi = 0°$ and (c) $\phi = 8°$ for an electron impact energy of 1200 eV. (d) The binding-energy spectrum of thiophene over all ϕ angles at an electron impact energy of 1200 eV. The dashed lines represent Gaussian fits to the peaks, and the solid line is the summed fit.

ADC(3) calculations have been carried out using Dunning's correlation-consistent polarized valence basis set of double-ζ quality (cc-pVDZ).[72] To assess the effect of diffuse functions on Dyson orbital momentum distributions, an attempt to use the aug-cc-pVDZ basis with diffuse functions centered on hydrogen, carbon, and sulfur atoms was also made. However, severe linear dependencies resulting in divergency problems prevented us from completing successfully ADC(3) calculations with the latter basis set. These led us to drop d-type diffuse functions on the sulfur atom, as well as d- and p-type diffuse functions on the carbon atoms, in the original aug-cc-pVDZ basis set, giving birth to a slightly smaller diffuse basis set referred to as the cc-pVDZ+ one.

The ionization spectra presented in the sequel have been simulated using as convolution function a combination of a Gaussian and a Lorentzian with equal weight (Voigt profile) and a constant full width at half of maximum parameter (fwhm) of 0.6 eV. The parameter has been selected in order to enable comparisons with available experimental data obtained by means of synchrotron radiation photoelectron spectroscopy (SRPES). Spherically averaged orbital momentum distributions have been generated from the output of 1p-GF/ADC(3) or DFT calculations using the MOMAP program by Brion and co-workers,[73] homemade interfaces and G03-NEMS.[35,74] For comparison purposes, the theoretical spherically averaged momentum distributions that are discussed in this work have been convoluted with the experimental momentum resolution using Monte Carlo methods,[75] according to an experimental electron momentum resolution of $\Delta\phi = \pm 0.84°$, $\Delta\theta = \pm 0.53°$.[35]

In the present work, all experimental electron momentum distributions have been rescaled using a constant renormalization factor, obtained by comparing experimental results with summed ADC(3)/cc-pVDZ+ electron momentum distributions for the highest occupied molecular orbital (HOMO, $1a_2$ (**1**)) and the next occupied orbital, $3b_1$ (**2**). Despite the intricacy of the underlying vibrational structure for the $3b_1^{-1}$ ionization line,[52]

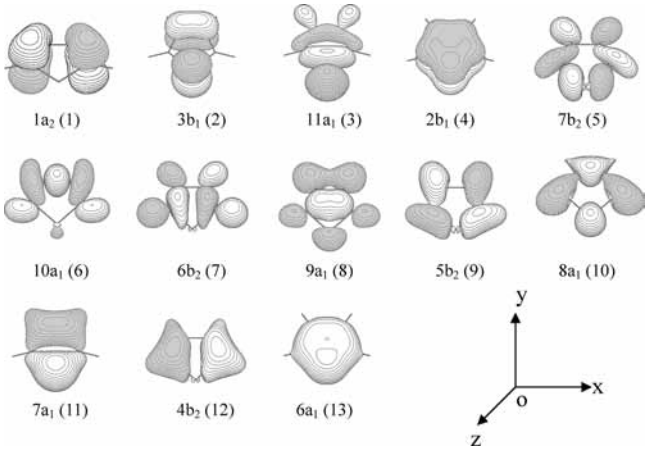

Figure 2. The valence molecular orbitals of thiophene [contour values: 0.05].

these two orbitals appear altogether in the SRPES measurements by D. M. P. Holland et al. (Figure 1a) as well as in our EMS measurements (Figures 1b−d) as one very sharp, intense, and well-isolated peak at 9.5 eV, and provide therefore altogether the best reference for a relative intensity scaling of the momentum distributions for all bands in the (e, 2e) ionization spectrum.

IV. Dyson Orbitals and Ionization Spectrum

At the HF/aug-cc-pVTZ level, thiophene in its ground state has, under the constraint of a C_{2v} symmetry point group, the following inner and outer valence shell electronic configurations:

inner valence shell: $\{(6a_1)^2\,(4b_2)^2\,(7a_1)^2\,(8a_1)^2(5b_2)^2\}$

outer valence shell:

$\{(9a_1)^2\,(6b_2)^2\,(10a_1)^2\,(7b_2)^2\,(2b_1)^2(11a_1)^2\,(3b_1)^2\,(1a_2)^2\}$

The topologies of the corresponding HF molecular orbitals are displayed in Figure 2. Four of the eight p-electrons delivered in the molecule by the four carbon atoms and one of the two electron lone pairs of the sulfur atom form a stable six-electron aromatic system characterized by three doubly occupied π-molecular orbitals ($1a_2$ (**1**); $3b_1$ (**2**) and $2b_1$ (**4**)), which are each characterized by a nodal surface that coincides with the plane of the ring. The outermost π-orbital, $1a_2$ (**1**), consists exclusively of C_{2p} contributions with antibonding relationships across the two symmetry planes of the molecule. In this orbital, maxima in electron densities coincide therefore with the two double bonds of the thiophene molecule. Orbital $3b_1$ (**2**) is an essentially nonbonding orbital that exhibits a significant S_{3p} contribution along the *y*-axis (Figure 2) and relates therefore dominantly to the so-called $n_S(\pi)$ electron lone pair that is involved in aromatic delocalization. The deepest π-orbital $2b_1$ (**4**) is fully delocalized on the ring and is the result of an all-bonding combination of $C_{2p(y)}$ and $S_{3p(y)}$ atomic orbitals. The remaining orbitals in the valence band belong all to the σ-band system and relate to C−C, C−S and C−H bonds. A stricter partitioning is in principle ruled out since all atomic orbitals contributing to this band system may interact with each other. Nonetheless, it can be seen that the $11a_1$ (**3**) orbital exhibits an important S_{3p} contribution along the main C_2 rotation axis (*z*-axis) of the molecule, and can therefore be ascribed to the second $n_S(\sigma)$ lone pair level. Also, orbitals $7b_2$ (**5**), $10a_1$ (**6**), $6b_2$ (**7**) and $9a_1$ (**8**) dominantly relate to the four C−H bonds of the molecule, whereas the inner-valence $5b_2$ (**9**), $8a_1$ (**10**), $7a_1$ (**11**), $4b_2$ (**12**) and $6a_1$ (**13**) orbitals correspond to the C−C and C−S bonds.

Our ADC(3) ionization spectra are displayed in Figure 3. In view of the selected width (fwhm) parameter for the spread function (0.6 eV), these convolutions may be readily compared with the SRPES measurements at a photon energy of 90 eV by D. M. P. Holland et al.[29] (Figure 1a). The reader is also referred to Table 1 for a detailed band assignment and comparison with further experimental and theoretical results. Five well-resolved one-electron ionization bands in the SRPES measurements by D. M. P. Holland on thiophene were explicitly assigned on the ground of similar ADC(3) calculations, although in conjunction with a smaller basis set, as well as through a determination of photoelectron asymmetry and branching ratio parameters. In order to prepare the analysis of electron momentum distributions throughout the valence region, we need to comparatively extend the assignment to all visible bands in the valence SRPES and EMS measurements on thiophene. In the present work, we therefore also focus on issues of relevance for unraveling the electron momentum distributions of this compound, such as the extent of the shake-up bands, and the influence on these bands of the employed basis set.

The one-electron picture of ionization prevails up to electron binding energies of 18.2 eV. Overall, the ADC(3) convolutions quantitatively match, within ∼0.2 eV to ∼0.3 accuracy, the experimental SRPES records up to electron binding energies of 21 eV. Both in the experimental spectra and the theoretical ADC(3) simulations, a rather pronounced depletion of intensities at ∼17.5 eV defines a rather clear border between the inner- and outer-valence regions (orbitals **1**−**8** and **9**−**13**, respectively). As usual, highly significant band broadenings on the experimental side (Figure 1, see also the EMS band widths in Table 1) corroborate the idea of a complete breakdown of the molecular orbital picture of ionization in the inner-valence region. Several rather intense shake-up lines ($\Gamma > 0.1$) also emerge in the outer-valence region, where the shake-up onset (S_1) corresponding to the $HOMO^{-2}\ LUMO^{+1}$ ($1a_2^{-2}\ 4b_1^{+1}$) transition in the π-band system is located at 13.83 eV (Table 1). The second shake-up line (S_2) at 15.5 eV (Table 1) also belongs to the π-band system and relates dominantly to the $(HOMO\text{-}1)^{-2}\ LUMO^{+1}$ ($3b_1^{-2}\ 4b_1^{+1}$) transition. The S_1 transition is too close to the one-electron ionization lines produced by the $7b_2$ (**5**) and $10a_1$ (**6**) orbitals to be directly discernible in a classical photoelectron experiment. On the other hand, although this was long deemed an uninteresting feature, the S_2 ($\pi^{-2}\pi^{*+1}$) satellite clearly emerges as a rather sharp peak at 15.5 eV in the experimental photoelectron spectrum displayed in Figure 1a or that by Kishimoto et al.[25] at 15.66 eV. Note that the S_1 and S_2 lines are not very much sensitive to the basis set (Figure 3).

The vertical double-ionization energy threshold of thiophene is located at ∼26.18 eV, according to benchmark CCSD(T)/aug-cc-pVTZ calculations. Therefore, all computed shake-up states at binding energies above this threshold are subject to decay via the spontaneous emission of a second electron and should be regarded as resonances in a continuum of shake-off states. Such states are therefore extremely sensitive to improvements of the basis set, in particular to the inclusion of diffuse functions. Enlarging the basis set leads typically to a redistribution of the shake-up ionization intensity over many more lines of weaker intensity. Due to the limitation of our exploration of the ADC(3) ionization spectrum to lines with a pole strength larger than 0.005, this intensity redistribution leads in turn to a

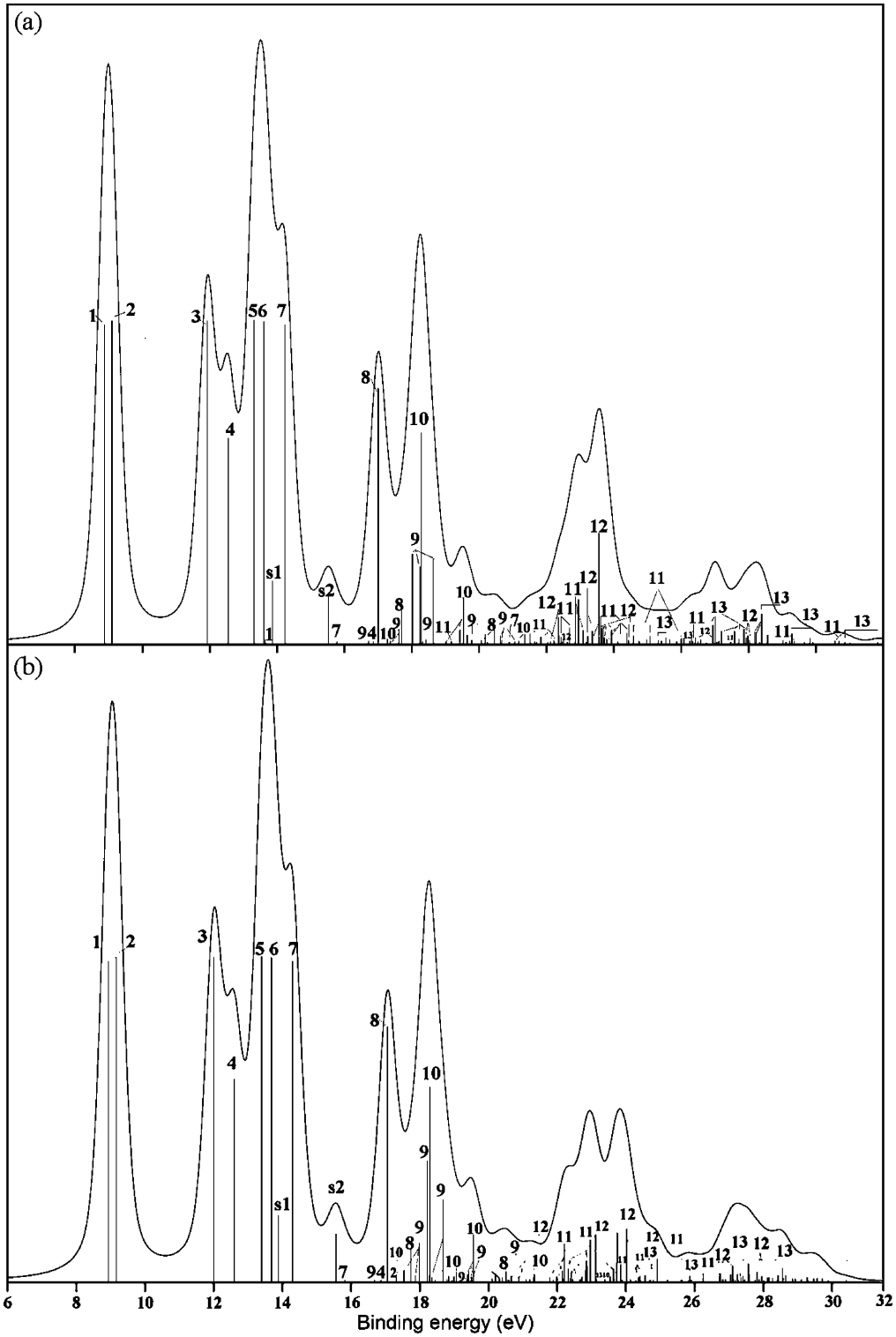

Figure 3. Theoretical ADC(3) spike spectra and convoluted densities of states (fwhm = 0.6 eV) obtained using the (a) cc-pVDZ and (b) cc-pVDZ+ basis sets.

significant lowering of spectral intensities and alterations of the shape of bands at electron binding energies larger than 23.5 eV. In contrast, the convoluted ADC(3) spectra are essentially insensitive to the basis set at electron binding energies lower than 23.5 eV, and provide therefore a robust enough theoretical basis on which to carry out our interpretation of EMS measurements. For instance, a shake-up line that distinctly emerges within the σ-band system in both theoretical spectra (Figure 3) is a satellite at 19.6 eV ($\Gamma = 0.13$) of the $8a_1^{-1}$ ($\mathbf{10}^{-1}$) one-electron ionization line at 18.3 eV ($\Gamma = 0.54$). This satellite may explain the shoulder seen at 19 eV in the SRPES measurements by D. M. P. Holland (Figure 1a). As shall be shown further, the influence of this line is more easily recognizable in EMS experiments.

Often, within the Born−Oppenheimer and harmonic approximations, the center of gravity of an electronic band is a good approximation to the corresponding vertical transition energy. However, strong vibronic coupling interactions associated with the presence of conical intersections of potential energy surfaces can lead to a collapse of the Born−Oppenheimer

TABLE 1: The Experimental and Theoretical Assignment of Ionization Spectra for Thiophene[a]

level	state[i]	He I UPS[b]	He I+II PES[c]	SR PES[d]	SR PES[e,f]	EMS[g]	SAC-CI[h]	ADC(3)[e]	ADC(3)/ cc-pVDZ[g]	ADC(3)/ cc-pVDZ+[g]	OVGF/ aug-cc-pVTZ[g]	B3LYP/ aug-cc-pVTZ[g]
1	$1a_2$ (π_3)	8.96	8.87	9.0	8.9	9.00[0.90]	8.92 (0.90)	8.84 (0.88)	8.88 (0.88)	8.93 (0.88)	9.04 (0.90)	6.70
2	$3b_1$ (π_2)	9.58	9.52	9.5	9.6	9.48[0.80]	9.05 (0.89)	9.06 (0.89)	9.10 (0.90)	9.16 (0.89)	9.36 (0.90)	7.04
3	$11a_1$	12.04	12.1	12.0	12.1	12.09[1.35]	11.70 (0.87)	11.91 (0.88)	11.93 (0.90)	12.00 (0.89)	12.09 (0.89)	9.47
4	$2b_1$ (π_1)	12.49	12.7	12.5	12.6		12.56 (0.61)	12.52 (0.57)	12.55 (0.57)	12.59 (0.56)	12.98 (0.83)	10.51
	S_1						14.78 (0.08)	13.83 (0.15)	13.87 (0.18)	13.88 (0.18)		
	S_2	15.66			15.5	15.40[0.44]	16.19 (0.11)	15.46 (0.12)	15.53 (0.13)	15.56 (0.13)		
5	$7b_2$	13.15	13.3	13.2	13.3		13.32 (0.87)	13.35 (0.89)	13.32 (0.90)	13.39 (0.89)	13.35 (0.90)	10.65
6	$10a_1$	13.71	13.9	13.9	13.8	13.60[1.96]	13.41 (0.85)	13.60 (0.89)	13.62 (0.90)	13.68 (0.89)	13.56 (0.89)	10.88
7	$6b_2$	14.26	14.3	14.4	14.4		14.16 (0.86)	14.20 (0.88)	14.24 (0.88)	14.30 (0.88)	14.24 (0.89)	11.41
8	$9a_1$	16.52	16.6	16.6	16.6	16.30[0.90]	16.84 (0.72)	16.95 (0.70)	17.00 (0.71)	17.06 (0.70)	17.13 (0.85)	14.17
9	$5b_2$[i]	17.62	17.6	17.6	17.6	17.30[2.20]	18.05 (0.50)	17.97 (0.16)	18.02 (0.25)	17.99 (0.11)		15.16
							18.45 (0.05)	18.20 (0.27)	18.24 (0.22)	18.21 (0.33)		
							18.85 (0.06)	18.62 (0.16)	18.64 (0.24)	18.67 (0.23)		
10	$8a_1$[i]	18.3	~18.3	18.4	18.3	19.66[1.95]	18.07 (0.47)	18.09 (0.39)	18.28 (0.59)	18.29 (0.54)		15.50
							19.24 (0.09)	18.28 (0.10)	19.53 (0.13)	19.57 (0.13)		
11	$7a_1$[i]		~22.1	20.8	21.2	21.95[2.40]	22.39 (0.07)	22.08 (0.12)		22.21 (0.11)		19.84
							22.50 (0.08)	22.79 (0.08)	22.86 (0.13)	22.96 (0.12)		
12	$4b_2$[i]		~22.3	22.1	22.2		22.38 (0.06)	23.15 (0.08)	22.95 (0.13)	23.11 (0.13)		20.09
						24.05[1.80]	23.29 (0.32)	23.75 (0.08)	23.55 (0.31)	23.74 (0.14)		
										24.02 (0.15)		
13	$6a_1$[i]					26.21[2.60]	28.79 (0.04)	26.54 (0.04)	27.00 (0.07)	27.10 (0.05)		24.05
							28.89 (0.04)	28.17 (0.06)	28.38 (0.09)	27.56 (0.05)		

[a] Binding energies are given in eV, along with spectroscopic strengths (or pole strengths Γ_n) given in brackets. The widths of these Gaussian peaks are listed in square brackets. [b] See ref 25. [c] See ref 26. [d] See ref 28. [e] See ref 29. [f] Our assignment. [g] The present work. [h] See ref 49. [i] Breakdown of the orbital picture of ionization. Additional ADC(3)/cc-pVDZ shake up lines: $1a_2$ (**1**): 13.654 (0.012); $3b_1$ (**2**): 17.281 (0.010); $2b_1$ (**4**): 16.855 (0.007), 18.276 (0.019); $6b_2$ (**7**): 15.774 (0.008); $9a_1$ (**8**): 17.694 (0.094), 20.067 (0.010), 20.458 (0.042); $5b_2$ (**9**): 16.715 (0.009), 17.361 (0.008), 17.613 (0.041), 18.321 (0.008), 18.420 (0.013), 19.779 (0.011), 20.177 (0.028), 20.245 (0.005), 20.630 (0.024), 20.671 (0.011), 21.057 (0.008), 21.699 (0.006); $8a_1$ (**10**): 17.275 (0.016), 19.013 (0.008), 19.429 (0.040), 19.641 (0.026), 21.174 (0.008), 21.352 (0.028); $7a_1$ (**11**): 19.170 (0.009), 21.513 (0.030), 21.648 (0.007), 21.830 (0.021), 22.116 (0.007), 22.358 (0.076), 22.427 (0.020), 22.616 (0.006), 22.679 (0.045), 22.937 (0.077), 23.087 (0.040), 23.368 (0.019), 23.608 (0.078), 23.632 (0.044), 23.788 (0.015), 23.932 (0.040), 24.116 (0.008), 24.385 (0.031), 24.576 (0.023), 24.748 (0.009), 24.976 (0.012), 25.070 (0.022), 25.656 (0.012), 25.863 (0.008), 26.001 (0.016), 26.327 (0.009), 27.056 (0.006), 27.466 (0.005), 29.105 (0.007), 29.352 (0.009), 30.561 (0.009), 30.855 (0.005); $4b_2$ (**12**): 21.844 (0.019), 22.032 (0.006), 22.212 (0.010), 22.231 (0.007), 22.376 (0.023), 4b2 22.462 (0.007), 22.506 (0.012), 22.851 (0.007), 23.224 (0.022), 23.357 (0.037), 23.685 (0.051), 23.714 (0.019), 23.784 (0.011), 23.927 (0.038), 24.434 (0.011), 26.494 (0.008), 26.570 (0.013), 26.930 (0.016), 27.118 (0.009), 27.924 (0.018), 28.024 (0.011); $6a_1$ (**13**): 20.896 (0.007), 23.186 (0.006), 25.319 (0.012), 25.411 (0.011), 25.539 (0.018), 26.072 (0.018), 26.256 (0.010), 26.303 (0.028), 26.419 (0.018), 26.741 (0.005), 26.939 (0.053), 27.188 (0.038), 27.581 (0.036), 27.709 (0.015), 27.972 (0.024), 28.181 (0.035), 28.219 (0.033), 28.324 (0.006), 28.545 (0.009), 28.562 (0.026), 29.020 (0.011), 29.221 (0.010), 29.287 (0.030), 29.650 (0.006), 29.818 (0.016), 29.910 (0.006), 30.679 (0.009), 31.006 (0.005), 31.830 (0.006), 31.993 (0.005). Additional ADC(3)/cc-pVDZ+ shake up lines: $1a_2$ (**1**): 13.677 (0.012); $3b_1$ (**2**): 17.314 (0.010); $2b_1$ (**4**): 16.868 (0.007), 18.281 (0.019); $6b_2$ (**7**): 15.818 (0.008); $9a_1$ (**8**): 17.735 (0.093), 20.107 (0.010), 20.405 (0.015), 20.514 (0.031); $5b_2$ (**9**): 16.685 (0.008), 17.535 (0.034), 17.871 (0.020), 18.354 (0.015), 18.841 (0.016), 19.368 (0.009), 19.508 (0.015), 20.202 (0.023), 20.317 (0.010), 20.668 (0.020), 21.097 (0.008); $8a_1$ (**10**): 17.317 (0.016), 18.453 (0.008), 18.789 (0.009), 18.938 (0.006), 18.992 (0.016), 19.064 (0.029), 19.403 (0.023), 19.431 (0.030), 19.474 (0.005), 20.576 (0.008), 21.193 (0.009), 21.310 (0.014), 21.332 (0.023), 23.382 (0.009), 23.647 (0.011); $7a_1$ (**11**): 21.097 (0.006), 21.785 (0.015), 21.988 (0.017), 22.414 (0.033), 22.453 (0.009), 22.679 (0.010), 22.716 (0.016), 22.819 (0.034), 22.873 (0.047), 22.881 (0.006), 23.543 (0.017), 23.723 (0.053), 23.848 (0.050), 23.871 (0.007), 24.020 (0.037), 24.129 (0.009), 24.287 (0.006), 24.405 (0.017), 24.554 (0.021), 24.908 (0.065), 25.211 (0.007), 25.603 (0.007), 25.626 (0.006), 25.824 (0.006), 26.252 (0.027); $4b_2$ (**12**): 20.582 (0.006), 20.884 (0.015), 21.879 (0.007), 22.150 (0.032), 22.191 (0.009), 22.323 (0.038), 22.368 (0.013), 22.650 (0.007), 22.841 (0.054), 22.870 (0.025), 23.632 (0.039), 23.895 (0.008), 24.366 (0.014), 24.724 (0.007), 26.741 (0.021), 27.114 (0.007), 27.274 (0.005), 27.357 (0.015), 27.872 (0.010), 28.004 (0.006), 6a1 (13), 23.141 (0.009), 24.418 (0.005), 24.692 (0.007), 24.798 (0.007), 25.862 (0.018), 25.901 (0.007), 25.638 (0.007), 26.732 (0.026), 26.820 (0.009), 26.893 (0.009), 27.052 (0.022), 27.096 (0.007), 27.132 (0.009), 27.195 (0.008), 27.252 (0.023), 27.405 (0.017), 27.456 (0.008), 27.592 (0.024), 27.767 (0.007), 27.821 (0.029), 27.954 (0.018), 28.120 (0.014), 28.168 (0.015), 28.271 (0.012), 28.402 (0.007), $6a_1$ (**13**): 28.433 (0.019), 28.555 (0.039), 28.581 (0.011), 28.655 (0.020), 28.848 (0.010), 28.929 (0.010), 29.110 (0.008), 29.272 (0.015), 29.307 (0.006), 29.454 (0.010), 29.476 (0.011), 29.569 (0.012), 29.712 (0.011), 29.731 (0.009), 29.887 (0.007), 30.414 (0.008).

approximation, and give rise therefore to rather severe discrepancies between the experimentally apparent and the vertical transition energies. For thiophene, the $^2A_2$ (π_3^{-1}) photoelectron band by Derrick et al.[26] is characterized by a sharp 0−0 vibrational onset at 8.9 eV followed by an easily discernible vibrational progression. In sharp contrast, the $^2B_1$ (π_2^{-1}) photoelectron band shows no resolved structure and appears as a broad bump extending over more than 0.5 eV and culminating at 9.5 eV, a value to compare with benchmark theoretical estimates (SAC-CI, ADC(3)) ranging from 9.05 to 9.16 for the corresponding vertical ionization energy. As is well-known,[76] a broad, diffuse spectral band or an irregular vibrational structure is often the characteristic signature of nonadiabatic effects, which formally require extensive theoretical treatments beyond the Born−Oppenheimer and Franck−Condon approximations. To be more specific, and to prepare the reader to our forthcoming analysis of electron momentum distributions for the outermost ionization bands, it is important to note that the shape of the $^2B_1$ (π_2^{-1}) photoelectron band could be quantitatively interpreted as the result of vibronic coupling interactions with the $^2A_2$ (π_3^{-1}) state, using the linear vibronic coupling model,[51] as well as OVGF estimates of vertical ionization energies. Such effects therefore fully explain a rather significant underestimation, of the order of 0.4 eV, of the electron binding energy that is experimentally inferred for the $3b_1$ orbital by the best results that are available for the vertical ionization energy. As shall be seen in the sequel, the ultrafast nuclear dynamics that is induced

by vibronic coupling interactions is also likely to affect the associated electron momentum distributions.

The next noticeable feature that appears in the SRPES measurements (Figure 1a, ref 28) is a composite spectral band extending from 12 to 15 eV, and exhibiting three peaks and one shoulder at 12.0, 12.5, 13.2 and 13.9 and 14.4 eV. These essentially correspond to one-electron ionization lines originating from the $11a_1$ (**3**), $2b_1$ (**4**), $7b_2$ (**5**), $10a_1$ (**6**), and $6b_2$ (**7**) orbitals, respectively. Beyond the S_2 peak at 15.5 eV (Table 1, ref 29) that is ascribable to a satellite produced by ionization of the π-orbital $2b_1$ (**4**), we encounter at 16.6 eV the only band in the SRPES measurements on thiophene that corresponds to a single ionization line, due to orbital $9a_1$ (**8**), and which defines the border of the outer-valence region. In line with the simulations, this band is experimentally sharp, although the obtained pole strengths ($\Gamma = 0.70$ to 0.72) indicate that the corresponding $^2A_1$ photoelectron band in the He I photoelectron spectrum by Derrick et al.[26] shows a rather well-defined vibrational progression extending from 16.4 to 16.8 eV and beyond, that has been ascribed in terms of "ring-breathing" and "hydrogen-breathing" vibrations. These early views are consistent with the topology of the $9a_1$ (**8**) orbital (Figure 2). Vibrational complications and particularly strong geometrical relaxation effects must therefore explain a stronger discrepancy between the theoretical vertical ionization energy of 16.84 to 17.00 eV for the $9a_1$ (**8**) orbital and the experimental (He I UPS) adiabatic value of 16.3 eV for the associated 0−0 vibrational onset (see Figure 3 in ref 26).

As we now enter the inner-valence region subject to an extensive shake-up contamination, the $9a_1$ (**8**) band is followed by a comparatively broader and asymmetric spectral band produced by one-electron and satellite lines due to ionization of the $5b_2$ (**9**) and $8a_1$ (**10**) orbitals. In line with the amplification of the dispersion of the ionization intensity over shake-up lines, band broadening intensifies when continuing the investigation of the ionization spectrum toward the innermost levels (Table 1). In view of the obtained ADC(3) results, the peak maximum at 22.1 eV within the next spectral band can be ascribed to a few rather intense shake-up lines originating from the $4b_2$ (**12**) orbital, whereas the shoulder at about 20.8 eV in the SRPES measurements is safely ascribable to a complex set of shake-up lines produced by orbital $7a_1$ (**11**). Ionization of orbital $6a_1$ (**13**) results in a very broad shake-up band culminating at 26.1 eV and followed, beyond the vertical double ionization threshold at 26.18 eV (*vide supra*), by a very long shake-off tail extending up to electron binding energies of, at least, 40 eV.

In the outer-valence region, Table 1 indicates that, at the 1p-GF/ADC(3) level, the extension of the cc-pVDZ basis set to the cc-pVDZ+ one results in shifts of the one-electron ionization energies by 0.01 to 0.06 eV only toward higher electron binding energies. Furthermore, it is nice to find out that the SAC-CI, ADC(3) and OVGF results for one-electron ionization energies and pole strength are in general very similar, although the OVGF results tend to yield poorer agreement with experiment. A comparison of OVGF and ADC(3) (or SAC-CI) results confirms the empirical rule (see refs 56 and references therein) that OVGF pole strengths smaller than 0.85 systematically corroborate a breakdown of the orbital picture of ionization at the ADC(3) (or SAC-CI) level, in the form of dispersion at this level of the ionization intensity over several shake-up lines with comparable strength.

In contrast with SAC-CI, ADC(3) or OVGF calculations, it is clear that Kohn−Sham orbital energies obtained from standard DFT calculations are not suited at all for providing reliable estimates of one-electron binding energies. Compared with experiment, these yield underestimations by 2 to 3 eV, as a result of the too rapid falloff of the B3LYP exchange correlation potential at large distances due to the incompleteness of the compensation to the self-interaction error. This observation amply justifies a systematic confrontation of Kohn−Sham orbital momentum distributions against benchmark many-body results derived from ADC(3) Dyson orbitals.

Since, in an exact theory of ionization, ionization cross sections formally relate to the squared transition moments involving the Dyson orbitals associated with the ionization states of interest, we display in Figure 4 contour plots of the electron density differences between normalized ADC(3) Dyson orbital densities and the corresponding HF (or KS) orbital densities. More specifically, these electron density differences have been computed as follows:

$$\Delta\rho^{HF}(\vec{r}) = \rho^{ADC(3)}(\vec{r}) - \rho^{HF}(\vec{r})$$
$$\Delta\rho^{KS}(\vec{r}) = \rho^{ADC(3)}(\vec{r}) - \rho^{KS}(\vec{r}) \quad (3)$$

with

$$\rho^{ADC(3)}(\vec{r}) = \left[\sum_n \Gamma_n\right]^{-1} \sum_n g_n^{\,2}(\vec{r}) \quad (4)$$

where the sums on n run on all identified ionization lines that could be recovered for a given HF molecular orbital. When the orbital picture of ionization is valid, these sums reduce to a single component only; otherwize, these sums imply an averaging of Dyson orbital densities over all the associated shake-up satellites. Upon a comparison of Figure 4 with Figure 2, it is rather clear that, compared with HF orbitals, electronic correlation in the Dyson orbitals characterizing the outermost ionization lines (**1**, **3**) tends to slightly increase the electron densities at remote distances and in antibonding regions associated with C_{3p} orbitals. This view is consistent with the dominance for such lines[77] of so-called electron *pair removal* (PRM) effects described by double electronic excitations from occupied to unoccupied HF orbitals.[78] At higher ionization energies, electron *pair relaxation* (PRX) effects described by a single electronic excitation from occupied to virtual orbitals along with a scattering of the electron hole tend to dominate the many-electron processes. Compared with the HF depiction, a decrease of the electronic densities in the region associated with the sulfur σ lone pair is therefore most generally observed with the associated Dyson orbitals. In contrast, electron transfers are usually reversed upon comparing Dyson orbital densities with KS orbital densities, at least upon considering the contributions from the lines (**1**−**3**, **5**−**9**) for which the one-electron picture of ionization is valid. For these lines, it appears therefore that the so-called target-Kohn-Sham (B3LYP) approximation for empirically computing Dyson orbital densities tends somehow to slightly overshoot many-body corrections for electronic correlation and relaxation.

V. Comparison between Experimental and Theoretical Momentum Distributions

Considering the results of our ADC(3) calculations and of the available PES measurements on thiophene, the angular resolved valence (e, 2e) ionization spectra obtained from this compound (Figure 1) have been deconvolved up to electron binding energies of about 30 eV, using a set of 11 Gaussian components (**I**−**XI**) and the SRPES estimates for the corresponding ionization energies, by means of a least-squares-fitting

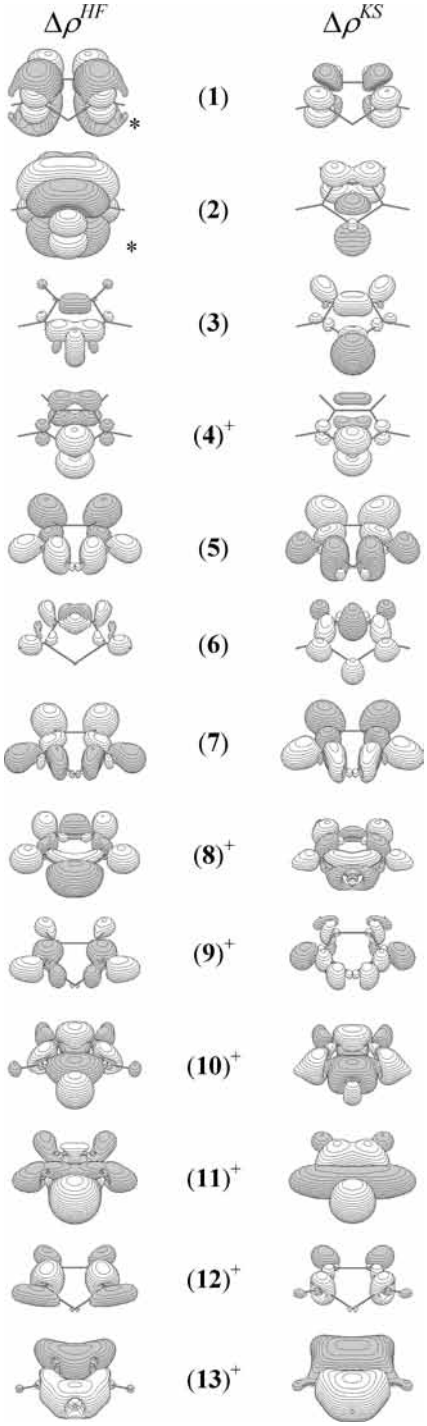

Figure 4. Contour plots of electron density differences ($\Delta\rho$) between normalized averaged Dyson orbitals and the related HF or KS orbitals (see text for explanation). The selected values for the contours are 0.001, except (*) for the $\Delta\rho^{HF}$ plots associated with orbitals $1a_2$ (**1**) and $3b_1$ (**2**), for which a contour value of 0.0001 was retained. The "+" superscripts emphasize a partial or complete breakdown of the orbital picture of ionization. The gray and white areas correspond to regions that exhibit an increase or decrease of the electron density, respectively.

technique. Analysis of the dependence of the ionization intensity recovered for each of these components enables us in turn to experimentally infer the associated electron momentum distribution. The widths of the Gaussian bands were estimated by combining the EMS instrumental energy resolution with the experimental (SRPES) widths of the vibrational (Franck−Condon) profiles. In this evaluation, small adjustments were also made in order to compensate for the asymmetries of some of these profiles. In Figure 1, the fitted individual Gaussian components are presented in the form of dashed lines while their sums fitting the ionization spectra are represented by solid lines.

In view of the obtained ADC(3)/cc-pVDZ and ADC(3)/cc-pVDZ+ results, the experimentally inferred electron momentum distributions for the fitted Gaussian components **I**−**XI** to the (e, 2e) ionization spectra were compared with theoretical results obtained by summing the spherically averaged ADC(3) Dyson orbital momentum distributions of all identified one-electron and shake-up ionization lines within the following energy intervals: **I**+**II**, [7.8−10.43 eV]; **III**, [10.43−13.03 eV]; **IV**, [13.03−14.80 eV]; **V**, [14.80−15.72 eV]; **VI**, [15.72−17.13 eV]; **VII**, [17.13−18.67 eV]; **VIII**, [18.67−20.41 eV]; **IX**, [20.41−22.84 eV]; **X**, [22.84−25.36 eV]; **XI**, [25.36−28.34 eV]. Although they rather strongly overlap in the EMS measurements, an attempt was also made to disentangle the contributions (**I**, **II**) from the two outermost orbitals [$1a_2$ (**1**), $3b_1$ (**2**)]. Therefore, in line with the ADC(3)/cc-pVDZ+ one-electron and shake-up ionization energies and the related transition moments, and to provide a consistent description of the experimental momentum distributions from the corresponding Dyson orbitals, the theoretical ionization intensity ascribed to the eleven identified Gaussian components in the EMS records has been partitioned as follows: **I**, $1a_2$ (**1**) [8.93 eV, $\Gamma = 0.881$]; **II**, $3b_1$ (**2**) [9.16 eV, $\Gamma = 0.892$]; **III**, $11a_1$ (**3**) [12.00 eV, $\Gamma = 0.892$]+ $2b_1$ (**4**) [12.593 eV, $\Gamma = 0.557$]; **IV**, $7b_2$ (**5**) [13.393 eV, $\Gamma = 0.894$] + $10a_1$ (**6**) [13.678 eV, $\Gamma = 0.891$] + S_1 (**4**) [13.882 eV, $\Gamma = 0.184$] + $6b_2$ (**7**) [14.300 eV, $\Gamma = 0.881$]; **V**, S_2 (**4**) [15.556 eV, $\Gamma = 0.134$]; **VI**, $9a_1$ (**8**) [17.056 eV, $\Gamma = 0.701$]; **VII**, $5b_2$ (**9**) [*, $\Gamma_{tot} = 0.753$] + $8a_1$ (**10**) [*, $\Gamma_{tot} = 0.597$]; **VIII**, $5b_2$ (**9**) [*, $\Gamma_{tot} = 0.166$] + $8a_1$ (**10**) [*, $\Gamma_{tot} = 0.239$]; **IX** , $7a_1$ (**11**) [*, $\Gamma_{tot} = 0.396$] + $4b_2$ (**12**) [*, $\Gamma_{tot} = 0.185$]; **X**, $7a_1$ (**11**) [*, $\Gamma_{tot} = 0.308$] + $4b_2$ (**12**) [*, $\Gamma_{tot} = 0.482$] + $6a_1$ (**13**) [*, $\Gamma_{tot} = 0.105$]; **XI**, $7a_1$ (**11**) [*, $\Gamma_{tot} = 0.027$] + $4b_2$ (**12**) [*, $\Gamma_{tot} = 0.064$] + $6a_1$ (**13**) [*, $\Gamma_{tot} = 0.548$]. In the latter list, S_1 and S_2 refer to the two outermost $\pi^{-2}\,\pi^{*+1}$ satellites with $\Gamma > 0.1$ due to the $2b_1$ (**4**) orbital (see preceding section), whereas asterisks emphasize that bands **VII** to **XI** at electron binding energies around 17.30, 19.66, 21.95, 24.05 and 26.21 eV correspond to highly congested sets of shake-up lines. For these bands, the reported total strength (Γ_{tot}) is the total fraction of ionization that could be recovered for each relevant orbital, by summing the contribution of all identified ionization lines within the corresponding range of electron binding energies (see above). The un-recovered fractions of ionization intensities are expected to contribute to very extended correlation tails,[79] consisting of many shake-up lines (and, by extension to the continuum, of shake-off bands) with very limited small strengths ($\Gamma < 0.005$). In order to enable meaningful comparisons with momentum distributions recovered from un-normalized Dyson orbitals, all the momentum distributions generated from KS orbitals have been rescaled according to the above listed values for the pole strengths (Γ) or total pole strengths (Γ_{tot}).

The angular resolved valence (e, 2e) ionization spectra of thiophene at $\phi = 0°$ and at $\phi = 8°$ are displayed in Figures 1b and 1c. By analogy with atomic orbitals, the associated momentum distribution profiles can be roughly divided into two types, referred to as s-type or p-type profiles, depending on the symmetry characteristics of the orbital. With an s-type profile, the maximum in electron density is found at $p \sim 0$ au, and the density decays overall exponentially with increasing values of p. Such orbitals are easy to identify in EMS experiments, since the associated bands emerge very prominently in the (e, 2e)

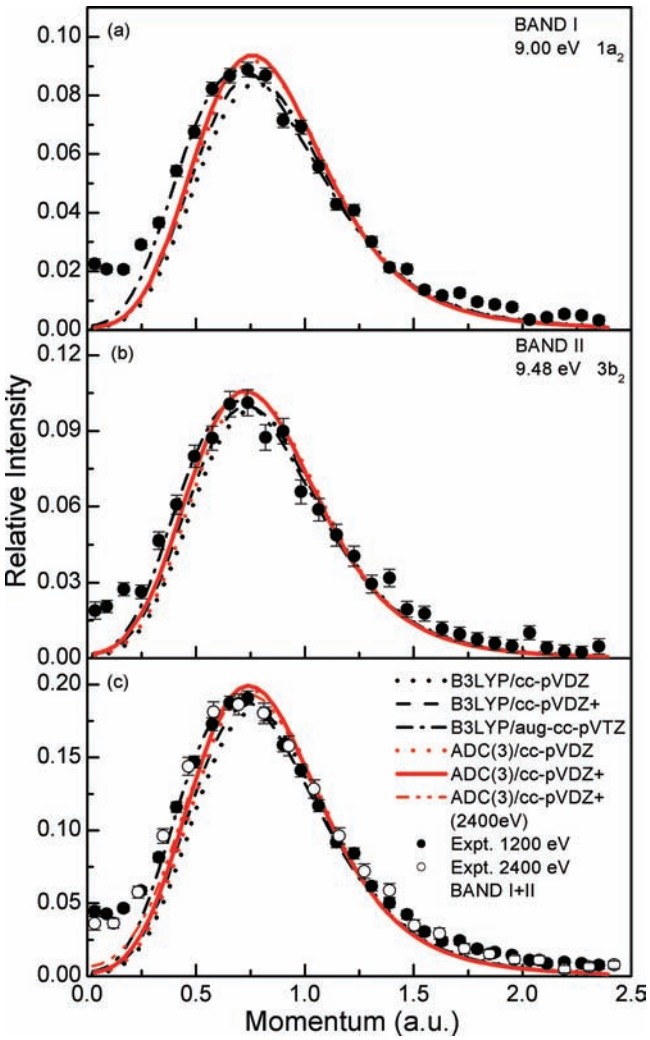

Figure 5. Experimental and calculated momentum distributions for bands **I**-$1a_2$ (**1**), **II**-$3b_2$ (**2**) and the summed band.

spectrum at $\phi = 0°$, whereas their relative intensity fades away upon increasing values of ϕ. A striking example for such a behavior in this work on thiophene is that of band **VI** (Figures 1b and 1c), which exclusively relates to the fully symmetric orbital $9a_1$ (**8**). Inversely, with a p-type profile the maximum in the electron density is found at a nonvanishing but finite value of p, whereas the density vanishes both at $p = 0$ and at $p \rightarrow \infty$. The two outermost valence bands related to the π-orbitals $1a_2$ and $3b_1$ belong to some extent to this category, since the associated bands (**I**, **II**) tend to vanish at $\phi = 0°$ (Figure 1b), and to dominate the spectrum at $\phi = 8°$ (Figure 1c).

The experimental momentum distributions for these two orbitals, located experimentally at 9.00 and 9.48 eV in the (e, 2e) ionization spectra of Figures 1b−d, are shown in Figures 5a and 5b, respectively, along with the results of various DFT and ADC(3) calculations. According to all these calculations in a rigid molecular framework, these orbitals exhibit a p-type momentum distribution with the maximum in the electron density located around $p = 0.74$ au for the $1a_2$ orbital (band **I**), and $p = 0.73$ au for the $3b_2$ orbital (band **II**). It can also be seen that, both from an experimental and from a theoretical viewpoint, these two orbitals exhibit very similar momentum profiles, hence their discrimination on experimental grounds is rather problematic. With either the individual (Figures 5a and 5b) or summed (Figures 5c) contributions from bands **I** and **II**, all theoretical calculations fail to reproduce a significant turn-up of the (e, 2e) ionization intensities at momenta below 0.3 au. Because of this turn-up, which enters the normalization factor used to rescale electron momentum distributions, the fact that the B3LYP momentum distributions slightly better reproduce the experiment at larger values of p should therefore be regarded as somehow artificial. Note that all calculations produce essentially the same results, and are not very much sensitive to improvements of the cc-pVDZ basis set. The $1a_2$ and $3b_2$ ionization lines are very well isolated from other cationic states in the ionization spectrum, and it is therefore extremely unlikely that the discrepancies that are observed between theory and experiment at low electron momenta for the composite band **I**+**II** (Figure 5c) are due to overlap effects from other Gaussian components in the deconvolution procedure. These discrepancies are partly due to a breakdown of the plane wave impulse approximation, i.e., distorted wave effects, which are typically encountered[15] with molecular or atomic orbitals exhibiting a π*-type or d-type topology, respectively (note indeed from Figure 2 that both the $1a_2$ and $3b_1$ orbitals exhibit two perpendicular nodal surfaces). In line with this suggestion, it appears, upon inspection of Figure 5c, that the total electron momentum distribution for bands **I** and **II** is rather sensitive to the kinetic energy of the impinging electron (E_0), and that increasing the latter from 1200 to 2400 eV slightly improves the agreement with theory. However, although the plane wave impulse approximation is consensually regarded as valid at impact energies above 1600 eV, large discrepancies between theory and experiment still remain at low electron momenta when $E_0 = 2400$ eV. Lacking any better explanation, these discrepancies *must* therefore merely reflect a symmetry breaking due to vibronic interactions and ultrafast nuclear motions, the time scale of which should be typically of the order of a few fs. Note indeed that upon considering the time it takes for an electron with an energy of the order of 1 keV to cover distances ranging from a few angstroms to a few hundreds angstroms, the time scale that characterizes EMS experiments typically decreases from 10^{-17} s at $p = 1$ au to 10^{-15} s at $p = 0.01$ au. This implies that nuclear motions due to vibronic coupling interactions around conical intersections can be fast enough to be detectable experimentally from electron densities measured around the origin of momentum space, while they would remain undetectable at large electron momenta. Wave packet electron and nuclear dynamics calculations would be needed for quantitatively treating such effects in theoretical modelings of electron (e, 2e) ionization experiments. Similar "turn ups" in the (e, 2e) cross sections have also been observed for the outermost levels of furan and pyrrole,[80] and still lack at present a quantitative interpretation.

The EMS momentum distributions for the identified bands **III**−**V** are shown in Figure 6, whereas the underlying individual orbital contributions are drawn in Figure 7. The experimental profile for band **III** at ~12.09 eV (Figure 6a) is dominantly of the p-type and exhibits a maximum at ~0.41 au, as well as a shoulder at ~1.06 au, respectively. The latter shoulder is predominantly due to orbital $11a_1$ (**3**), the momentum distribution profile of which is given in Figure 7a. The presence of two minima, at $p = 0.00$ and $p = 0.79$ au, and of two maxima, at $p = 0.30$ and $p = 1.11$ au in this profile corroborates the presence of three nodal surfaces across the ring backbone of thiophene (Figure 2), with the main component at $p = 0.30$ being merely related to the peripheral lone-pair $n_S(\sigma)$ contribution to this orbital. Indeed, the effect of the electron confinement associated with this lone pair becomes more limited upon an incorporation of diffuse functions in the basis set, which

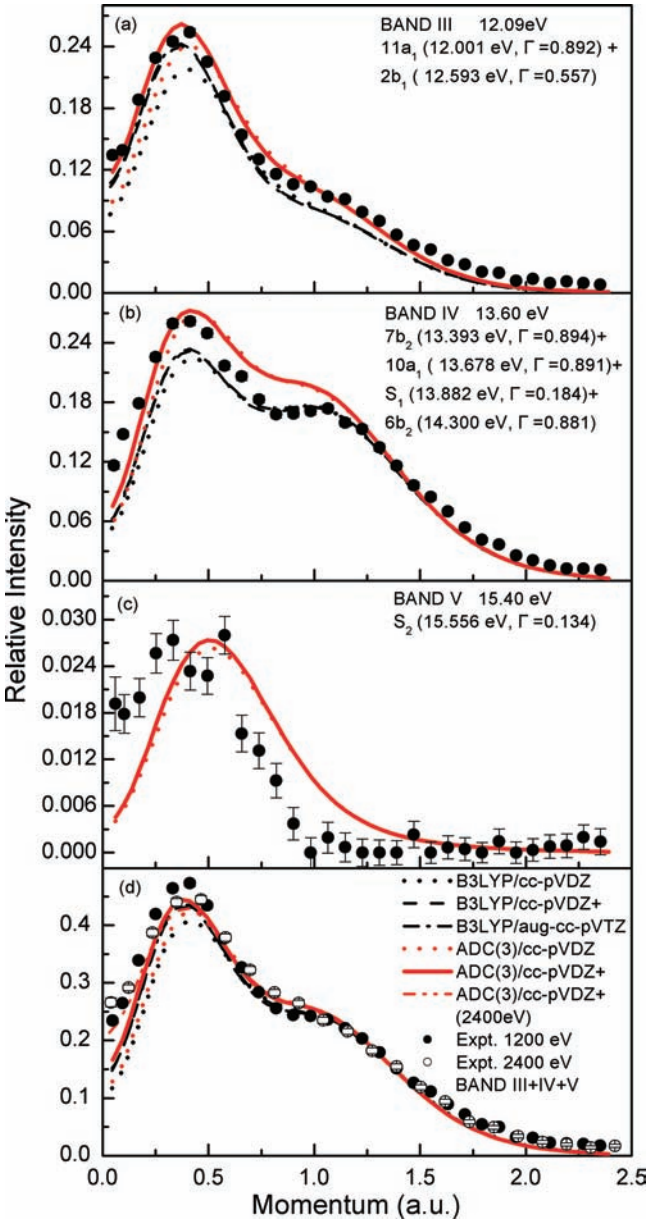

Figure 6. Experimental and calculated momentum distributions for bands **III**, **IV**, **V** and the summed band.

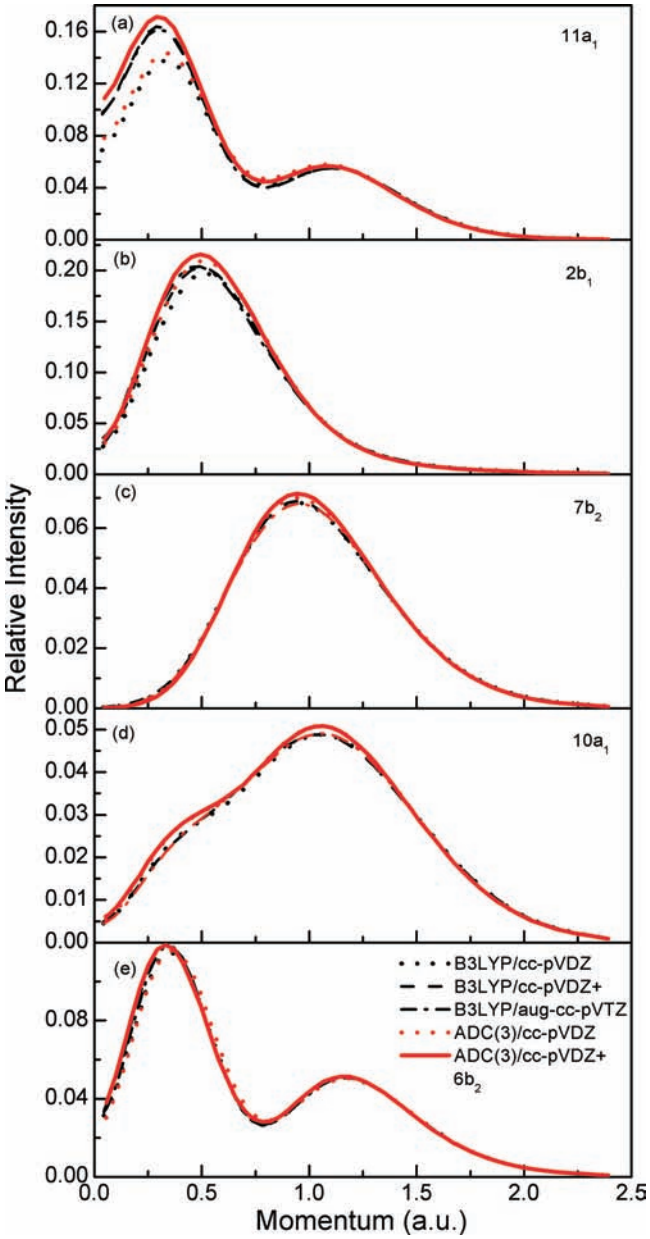

Figure 7. Theoretical momentum distribution profiles for the $11a_1$ (**3**), $2b_1$ (**4**), $7b_2$ (**5**), $10a_1$ (**6**) and $6b_2$(**7**) orbitals at various theoretical levels (individual Dyson orbital has been normalized).

correspondingly leads (Figures 6a and 7a) to a very pronounced rise of (e, 2e) intensities in the low momentum region ($p < 0.6$ au). Inspection of Figure 6a indicates therefore a generally excellent agreement between the experimental data and the calculated profiles, provided diffuse functions are included in the basis set, with the best theoretical insights being clearly provided by the ADC(3)/cc-pVDZ+ results. Since the underlying $2b_1$ (**4**) orbital is subject to a partial breakdown of the one-electron picture of ionization, this observation also confirms the high quality of the computed ionization pole strengths and Dyson orbitals, and demonstrates the relevance of our theoretical analysis so far. The innermost π-orbital $2b_1$ (**4**) of thiophene is a nicely delocalized orbital (Figure 2), with limited electron confinement therefore, and exhibits as a result its maximum in the corresponding p-type momentum distribution profile (Figure 7b) at a lower electron momentum value ($\sim$0.5 au) than the two outermost π-orbitals $1a_2$ (**1**) and $3b_2$ (**2**), the maximum density of which locates at $\sim$0.75 au (Figures 5a and 5b).

The electron momentum distributions obtained from band **IV** at 13.60 eV in the (e, 2e) ionization spectra are analyzed in Figure 6b. According to the ADC(3) depiction (Figure 3), this band encompasses one-electron contributions from the outer valence orbitals $7b_2$ (**5**), $10a_1$ (**6**), and $6b_2$ (**7**), as well as the $\pi^{-2}\ \pi^{*\ +1}$ satellite line $\mathbf{S_1}$ at 13.882 eV produced by the $2b_1$ (**4**) orbital. Since DFT calculations are not suited for coping with such states, the contribution of the $\mathbf{S_1}$ line was not accounted for when modeling the electron momentum distribution associated with band **IV** on the ground of B3LYP Kohn−Sham orbitals. Upon considering the p-type profile displayed in Figure 7b for the $2b_1$ (**4**) orbital, which exhibits its maximum at 0.50 au, it is clear from Figure 6b that the contribution from this satellite is directly recognizable in EMS as it helps to very substantially improve the agreement between the theoretical and experimental (e, 2e) cross sections at electron momenta around 0.5 au. The individual momentum distributions associated with the $7b_2$ (**5**) and $10a_1$ (**6**) orbitals are both essentially of the p-type (Figures 7c and 7d), with one major broad component around $p = 1$ au relating to the contribution from the peripheral C−H bonds (Figure 2), and for the latter orbital (Figure 7d), a

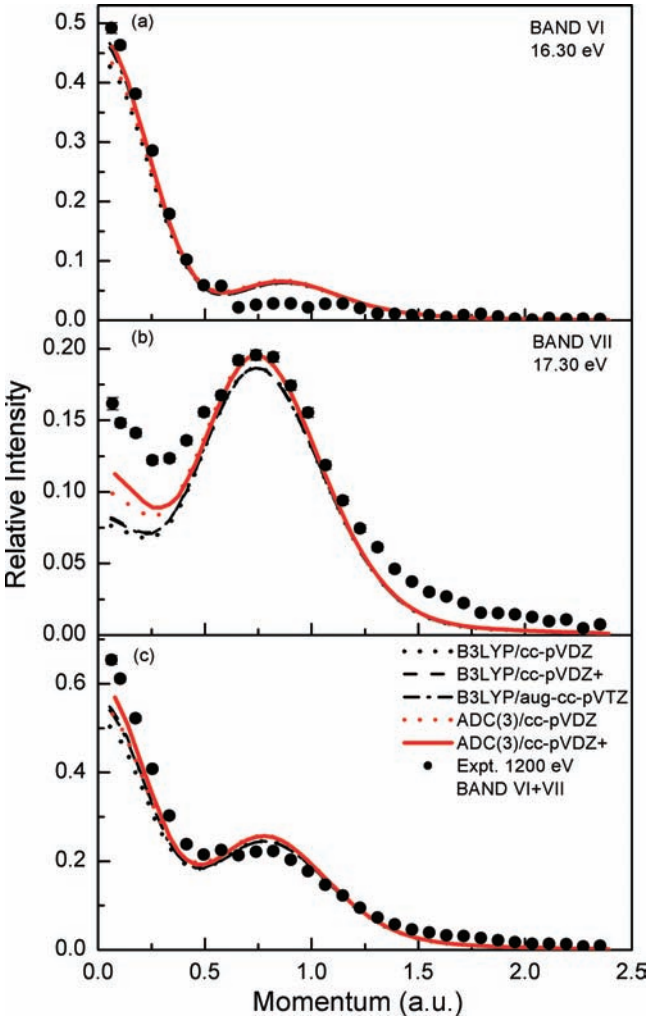

Figure 8. Experimental and calculated momentum distributions for bands **VI**, **VII** and the summed band.

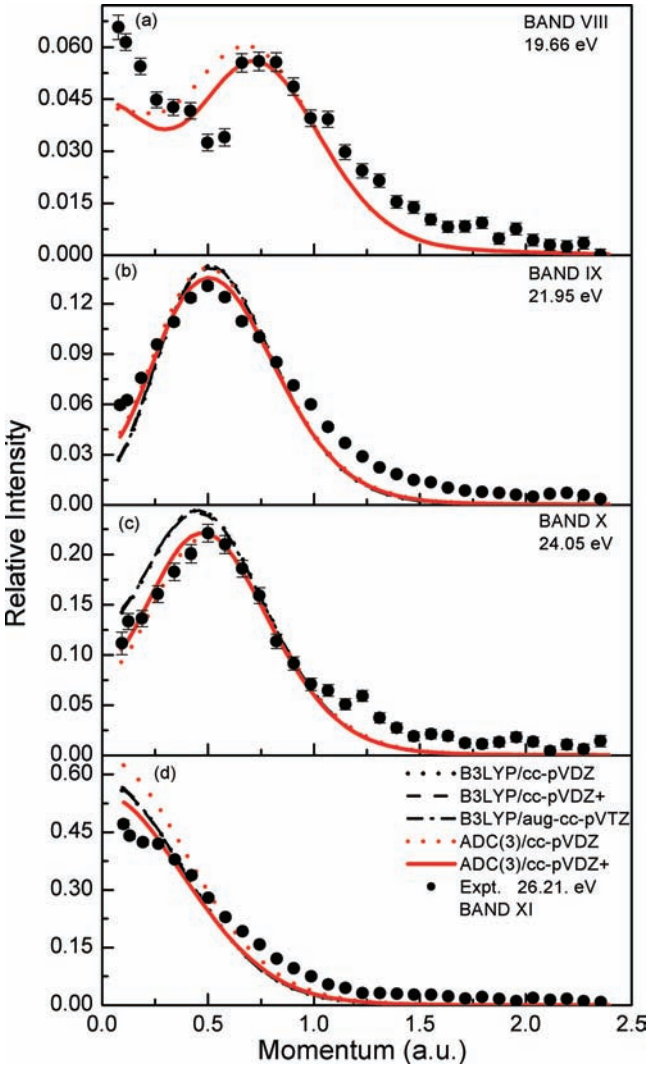

Figure 9. Experimental and calculated momentum distributions for bands **VIII**, **IX**, **X** and **XI**.

secondary minor component in the form of a shoulder at $p \sim 0.42$ au that can be associated with a more strongly localized C−C contribution (Figure 2). In contrast, the momentum distribution produced by the $6b_2$ (**7**) orbital (Figure 7e) exhibits two well-defined components, at $p = 0.33$ and 1.16 au, and its contribution to band **IV** is therefore rather easily recognizable. Compared with the low momentum component to the $11a_1$ (**3**) orbital (Figure 7a) dominantly associated with the $n_S(\sigma)$ lone pair, the momentum distributions for the $2b_1$ (**4**), $7b_2$ (**5**), $10a_1$ (**6**) and $6b_2$ (**7**) orbitals (Figures 7b−e) exhibit a much reduced dependence upon the basis set at low p values, which reflects their less diffuse nature and relationships to C−H bonds.

As is clearly shown from the SRPES measurements, the $\pi^{-2}\ \pi^{*\,+1}$ satellite line $\mathbf{S_2}$ at 15.56 eV in the ADC(3) spectrum that is also due to the $2b_1$ (**4**) orbital is sufficiently well isolated to be experimentally amenable on its own in EMS experiments. This satellite gives rise to band **V**, the electron momentum density of which is separately analyzed on the ground of ADC-(3) Dyson orbital calculations in Figure 6c. The corresponding electron momentum distributions are not very much dependent on the quality of the basis set, and there is clearly for this band a satisfactory enough match between theory and experiment to reliably confirm the presence of a second $\pi^{-2}\ \pi^{*\,+1}$ satellite around 15.40 eV in the (e, 2e) ionization spectra of thiophene.

Some discrepancies at electron momenta ranging from 0.6 to 1.0 au for band **IV** (Figure 6b) appear to be due to a non-negligible overlap (Figures 1b−d) with band **V**. Indeed, the discrepancies between theory and experiment almost entirely disappear upon summing the contributions of bands **III**, **IV** and **V** (Figure 6d), except at particularly low momenta ($p < 0.1$ au). In order to limit the extent of errors due to a partial failure of the plane wave impulse approximation, the theoretical ADC-(3)/cc-pVDZ+ momentum distribution associated with the composite band **III**+**IV**+**V** is compared in Figure 6d with EMS measurements at an electron impact energy of 2400 eV. It is clear from this comparison and from the latter figure that ADC-(3) is the best suited approach for investigating the experimental momentum distributions associated with these electron binding energies, particularly at electron momenta above 0.5 au. Also, diffuse functions appear here to be essential for quantitatively reproducing the experimental (e, 2e) ionization intensities in the momentum region below ~0.4 au. Lacking such functions leads indeed in this case to rather significant underestimations of electron densities at low values of p.

The EMS momentum distributions for the identified bands **VI**−**XI** are given in Figures 8 and 9, whereas the underlying individual orbital contributions are displayed in Figure 10. Band **VI**, at 16.30 eV, relates exclusively to a single one-electron ionization line due to orbital $9a_1$ (**8**), and its electron momentum distribution therefore rather faithfully reflects that from the latter orbital (Figure 8a). In line with the symmetry of this orbital, we experimentally observe an s-type profile with a very sharp

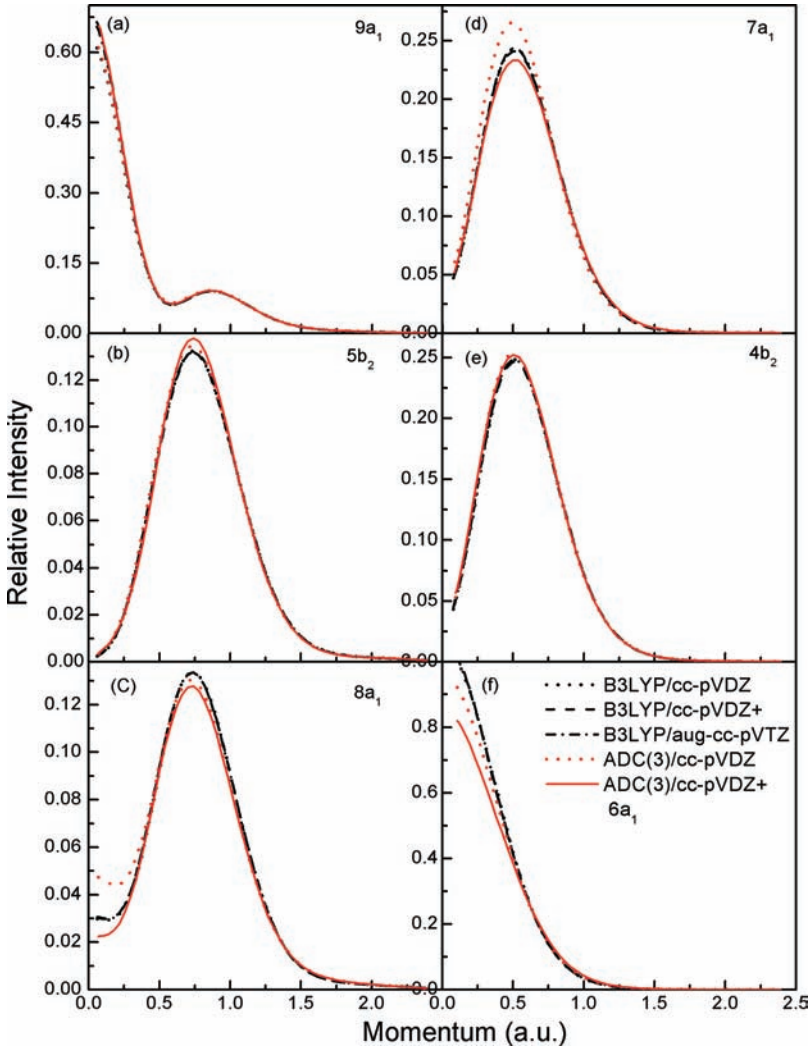

Figure 10. Theoretical momentum distribution profiles for the $9a_1$ (**8**), $5b_2$ (**9**), $8a_1$(**10**), $7a_1$ (**11**), $4b_2$ (**12**) and $6a_1$ (**13**) orbitals at various theoretical levels (individual Dyson orbital has been normalized).

component at $p = 0$ au, and weaker structures at $p = 0.89$ and 1.15 au which seem to corroborate a rather significant shoulder at p=0.88 in all theoretical momentum distributions. The presence of two well-defined maxima in the theoretical distributions, and thus of a minimum in the electron density at $p =$ 0.60 au, is the consequence of the confinement of the electron density due to one closed nodal surface that coincides with the ring formed by the carbon and sulfur atoms. Therefore, in view of the topology of the $9a_1$ (**8**) orbital, the peak at $p = 0.0$ au in the momentum profile reflects the contribution from the peripheral C−H bonds to this orbital, whereas the component around 0.88 au in the theoretical momentum distribution reflects weaker side-to-side and through-space bonding interactions between in-plane C_{2p} or S_{3p} atomic orbitals.

Beyond band **VI**, the one-electron picture ionization is no longer a valid concept, as we enter the inner-valence region which contributes to C−C and C−S bonds and which is subject to a severe shake-up contamination. Due to the more localized nature of the molecular orbitals from this energy region, the computed momentum profiles are in general not very much sensitive to the inclusion of diffuse functions in the cc-pVDZ basis set (Figure 10). Band **VII** at 17.3 eV is particularly broad (Table 1) and was ascribed to a dense set of ionization lines arising from orbitals $5b_2$ (**9**) and $8a_1$ (**10**), the momentum distributions of which are given in Figures 10b and 10c. The $5b_2$ (**9**) orbital yields a perfect p-type profile, whereas the $8a_1$ (**10**) orbital seems to exhibit a shallow maximum in the ADC(3)/cc-pVDZ+ distribution. Despite the complexity of the underlying shake-up set, the ADC(3) Dyson orbital momentum distributions fairly reproduce the trends that emerge from the experimental momentum profile inferred for band **VII** (Figure 8b), which exhibits two maxima at $p \sim 0$ au and $p = 0.74$ au, along with one minimum at 0.25 au. It is here also clear that the B3LYP results provide in the low momentum region ($p <$ 0.5 au) inferior insights into the experimental results. However, all theoretical calculations strongly underestimate the magnitude of the (e, 2e) cross sections characterizing band **VII** in the low momentum region. This discrepancy between theory and experiment is probably due to a large extent to overlap effects between bands **VI** and **VII**. In order to further investigate this "turn up" effect, the summed experimental (e, 2e) cross sections characterizing these two bands under electron impact energies of 1200 eV are compared with the summed theoretical momentum distributions for these two bands in Figure 8c. This time, in very reasonable agreement with experiment, all models correctly predict a mixed s-p-type momentum profile, which confirms the suggestion that the too severe rise of (e, 2e) ionization intensities for band **VII** near the origin of momentum space is the result of its overlap with band **VI**. Therefore, in line with our above observations for the minor component at $p = 0.74$ au in the momentum profile of band **VI,** one should notice

nonetheless that theory still overshoots the experimental (e, 2e) ionization intensities around $p = 0.78$ au in the summed profiles.

Like band **VII**, band **VIII** at 19.7 eV is also attributed to many satellites, but of considerably lower strengths ($\Gamma < 0.10$), due to orbitals $5b_2$ (**9**) and $8a_1$ (**10**), with this time a markedly smaller proportion of $5b_2$ (**9**) satellites. Compared with band **VII**, this change in the proportion of satellites results, according to our simulations (Figure 9a), into an enhancement of the first component at $p = 0$ relative to the second one at $p = 0.74$ au. This is, from a qualitative viewpoint, precisely what is seen experimentally (Figure 9a), although here again overlap effects with band **VII** certainly impede more quantitative insights. The weaker intensities of the shake-up lines in this energy region have also an immediately recognizable effect on the global intensity of band **VIII**, and on the scale therefore of the corresponding momentum distribution.

Bands **IX** and **X**, located at 22.0 and 24.1 eV, respectively, in the inner valence (e, 2e) ionization spectra of thiophene (Figures 1b−d), relate merely to particularly complex sets of shake-up lines originating from the $7a_1$ (**11**) and $4b_2$ (**12**) orbitals, as well as to a few satellites with extremely weak ionization intensities (i.e. pole strengths) due to the innermost orbital $6a_1$ (**13**). Very naturally therefore, the corresponding p-type momentum distributions corroborate experimentally the presence of one nodal surface in the $7a_1$ (**11**) and $4b_2$ (**12**) orbitals (Figure 2). Very clearly, the most accurate insights into these momentum distributions are again obtained with the ADC(3) Dyson orbital momentum distributions. Despite their rescaling according to the computed fractions of the $7a_1$ (**11**) and $4b_2$ (**12**) recovered at these energy ranges, the B3LYP Kohn−Sham orbital momentum distributions yield, whatever the basis set, to significant overestimations of the experimental (e, 2e) ionization intensities inferred for band **X** at electron momenta below 0.66 au. Note nonetheless that, for band **IX**, a minor turn-up of the (e, 2e) ionization intensities around the momentum origin still eludes a quantitative explanation, and is most probably the result of a weak overlap with the adjacent band **VIII**.

With band **XI**, observed at 26.21 eV, we approach the shake-off threshold of thiophene. Quantitative orbital reconstructions from this energy region are further complicated by the fact that the unrecovered correlation tails produced by the above lying $7a_1$ (**11**) and $4b_2$ (**12**) shake-up bands could also slightly contaminate this region. Despite these difficulties, the experimental s-type dependence of the (e, 2e) ionization intensities upon the electron momentum parameter indicates an almost exclusive relationship of this band with the innermost orbital $6a_1$ (**13**). Here again, the ADC(3)/cc-pVDZ+ Dyson orbital momentum distribution provides the most accurate insights into experiment. The slight deviations from experiment that are observed here are most likely the outcome of the above-mentioned correlation tails, which in 1p-GF ionization spectra consist typically of shake-up lines with particularly small strengths ($\Gamma < 0.005$) and can extend up to extremely high electron binding energies (60 eV of more).[79]

VI. Conclusions

One-particle Green's function (1p-GF) theory of ionization along with the benchmark third-order algebraic diagrammatic construction scheme [ADC(3)] has been used to analyze new measurements employing high resolution electron momentum spectroscopy of the electron density distributions and electron binding energy spectrum of thiophene over the whole valence region. These measurements were performed using a recently developed binary (e, 2e) electron momentum spectrometer with markedly improved energy, angular, and momentum resolutions ($\Delta E = 0.8$ eV, $\Delta\theta = \pm 0.53°$ and $\Delta\phi = \pm 0.84°$, i.e. $\Delta p = 0.069$ and 0.098 au at electron impact energies of 1200 and 2400 eV, respectively). A comparison of the experimental records against 1p-GF/ADC(3) calculations of the vertical ionization spectrum of thiophene and of the spherically averaged electron momentum distribution derived from the related Dyson orbitals has enabled us to greatly improve our understanding of the neutral valence wave function as well as the excited-state properties of the radical cation of this molecule, within the framework of a many-body theoretical treatment that explicitly copes with configuration interactions in the neutral and final cationic states. Despite the presence of numerous shake-up lines within the π- and σ-spectral bands in the outer-valence region, and the complete breakdown of the orbital picture of ionization in the inner-valence region, these orbitals were found to yield most generally remarkably accurate enough insights into the experimentally inferred orbital momentum distributions, on the basis of a partitioning of the (e, 2e) ionization intensity which is consistent with the computed ADC(3) ionization energies and pole strengths. The angular dependence of the (e, 2e) ionization intensities confirms in particular the presence of two rather intense $\pi^{-2}\ \pi^{*+1}$ shake-up lines at electron binding energies of 13.8 and 15.5 eV, with pole strengths equal to 0.18 and 0.13, respectively, which both borrow their intensity to the deepest π-orbital, $2b_1$.

In line with the high molecular symmetry point group (C_{2v}) of thiophene, which inhibits significant alterations of overlap densities due to configuration interactions in the initial and final states, Kohn−Sham orbitals obtained with the standard B3LYP functional and ADC(3) Dyson orbitals lead overall to qualitatively very similar momentum distributions. Nonetheless, a confrontation of theoretical results against experiment demonstrates in many cases the superiority of ADC(3) Dyson orbitals for quantitative studies of transition moments associated with one-electron and shake-up ionization bands. In a few cases, diffuse functions were found to have a limited but discernible influence on the computed electron momentum profiles. It is worth noticing that the influence of diffuse functions on the calculated electron momentum densities, whatever the type of profile, is generally much more limited with the Kohn−Sham momentum distributions, which seems to be a rather obvious consequence of the too fast decay of the B3LYP electronic potential at large distances.

One noticeable discrepancy between theory and experiment that still eludes at this stage a quantitative enough interpretation pertains to the electron momentum distributions associated with the two lowest $^2A_2$ (π_3^{-1}) and $^2B_1$ (π_2^{-1}) cationic states. The experimental distribution exhibits a significant turn-up of the (e, 2e) ionization intensities at low electron momenta, which all employed models embodied within a vertical depiction of ionization events fail to reproduce. Comparison of measurements performed at electron impact energies of 1200 and 2400 eV (+ electron binding energy) indicates furthermore that these levels are not subject to very sizable breakdowns of the plane wave impulse approximation. Therefore, lacking any better explanation, this discrepancy between theory and experiment seems to provide further indirect evidence for a fast symmetry lowering and nuclear dynamical effects due to vibronic coupling interactions between these two states, a suggestion that is in line with recent theoretical studies of the vibrational profiles of these two states in high resolution photoelectron spectroscopy experiments employing synchrotron radiation. More specifically, considerations on electron velocities and electron momenta lead to an

estimate of the order of one to a few tenths femtosecond for the time scale characterizing these motions.

To conclude, besides recommending ADC(3) for quantitatively deciphering highly congested ionization spectra, we advocate a systematic use of ADC(3) Dyson orbitals in further analyses of the angular dependence of (e, 2e) ionization intensities in EMS experiments, in order to safely identify complications such as alterations of the molecular conformation,[13] distorted wave effects,[15] nuclear dynamics,[76] or a dispersion of the ionization intensities into shake-up processes (see, e.g., refs 11, 13, 14, 36−40, 47, 55−61).

Acknowledgment. This work was supported by the National Natural Science Foundation of China under Contract No.10575062 and the Specialized Research Fund for the Doctoral Program of Higher Education under Contract No. 20050003084. The authors also acknowledge the financial support by the Fonds voor Wetenschappelijk Onderzoek-Vlaanderen (FWO), i.e., the Flemish branch of the Belgian National Science Foundation, and the Bijzonder OnderzoeksFonds (BOF) of the University of Hasselt, where Y.R.H. has been working 9 months (15 June 2006 to 14 March 2007) as a PhD student, thanks to a fellowship obtained within the framework of a bilateral program for scientific cooperation between Belgium (Flanders) and P. R. China. B.H. was a postdoctoral researcher at Hasselt University from 01 July to 31 December 2006. He acknowledges financial support from the Technical University of Budapest, Hungary, from 01 February to 30 April 2007, and from a DFT-network sponsored by the FWO-Vlaanderen (Belgium), from 01 May 2007 to 30 April 2008.

References and Notes

(1) McCarthy, I. E.; Weigold, E. *Rep. Prog. Phys.* **1991**, *54*, 789.

(2) (a) Brion, C. E. *Int. J. Quantum Chem.* **1986**, *29*, 1397. (b) Coplan, M. A.; Moore, J. H.; Doering, J. P. *Rev. Mod. Phys.* **1994**, *66*, 985. (c) McCarthy, I. E.; Weigold, E. *Rep. Prog. Phys.* **1988**, *51*, 299.

(3) Weigold, E.; McCarthy, I. E. *Electron Momentum Spectroscopy*; Kluwer Academic Plenum Publishers: New York, 1999.

(4) (a) Pickup, B. T. *Chem. Phys.* **1977**, *19*, 193. (b) Mc Weeny, R.; Pickup, B. T. *Rep. Prog. Phys.* **1980**, *43*, 1065. (c) Öhrn, Y.; Born, G. *Adv. Quantum Chem.* **1981**, *13*, 1. (d) Deleuze, M.; Pickup, B. T.; Delhalle, J. *J. Mol. Phys.* **1994**, *83*, 655. (e) Seabra, G. M.; Kaplan, I. G.; Zakrzewski, V. G.; Ortiz, J. V. *J. Chem. Phys.* **2004**, *121*, 4142. (f) Ning, C. G.; Ren, X. G.; Deng, J. K.; Su, G. L.; Zhang, S. F.; Knippenberg, S. and Deleuze, M. S. *Chem. Phys. Lett.* **2006**, *421*, 52.

(5) Perdew, J. P. *Phys. Rev. B* **1986**, *33*, 8822.

(6) (a) Becke, A. D. *J. Chem. Phys.* **1993**, *98*, 5648. (b) Lee, C.; Yang, W.; Parr, R. G. *Phys. Rev. B* **1998**, *37*, 785.

(7) Hamel, S.; Duffy, P.; Casida, M.; Salahub, D. R. *J. Electron Spectrosc. Relat. Phenom.* **2002**, *123*, 345.

(8) (a) Casida, M. E.; Jamorski, C.; Casida, K. C.; Salahub, D. R. *J. Chem. Phys.* **1998**, *108*, 4439. (b) Tozer, D. J.; Handy, N. C. *J. Chem. Phys.* **1998**, *109*, 10180. (c) Reimers, J.; Cai, Z.-L.; Bilić, A.; Hush, N. S. *Ann. N.Y. Acad. Sci.* **2003**, *110*, 235.

(9) Bawagan, A. D. O.; Brion, C. E. *Chem. Phys. Lett.* **1987**, *137*, 573.

(10) Bawagan, A. D. O.; Muller-Fiedler, R.; Brion, C. E.; Davidson, E. R.; Boyle, C. *Chem. Phys.* **1988**, *120*, 335.

(11) Knippenberg, S.; François, J. -P.; Deleuze, M. S. *J. Comput. Chem.* **2006**, *27*, 1703.

(12) (a) Zheng, Y.; Neville, J. J.; Brion, C. E. *Sci.* **1997**, *270*, 786. (b) Takahashi, M.; Matsuo, M.; Udagawa, Y. *Chem. Phys. Lett.* **1999**, *308*, 195. (c) Brion, C. E.; Young, J. B.; Litvinyuk, I. V.; Cooper, G. *Chem. Phys.* **2001**, *269*, 101. (d) Huang, Y. R.; Knippenberg, S.; Hajgató, B.; François, J.-P.; Deng, J. K.; Deleuze, M. S. *J. Phys. Chem. A* **2007**, *111*, 5879.

(13) (a) Deleuze, M. S.; Pang, W. N.; Salam, A.; Shang, R. C. *J. Am. Chem. Soc.* **2001**, *123*, 4049. (b) Deleuze, M. S.; Knippenberg, S. *J. Chem. Phys.* **2006**, *125*, 104309. (c) Knippenberg, S.; Huang, Y. R.; Hajgató, B.; François, J.-P.; Deng, J. K. *J. Chem. Phys.* **2007**, *127*, 174306.

(14) (a) Knippenberg, S.; Nixon, K. L.; Brunger, M. J.; Maddern, T.; Campbell, L.; Trout, N.; Wang, F.; Newell, W. R.; Deleuze, M. S.; François, J.-P.; Winkler, D. A. *J. Chem. Phys.* **2004**, *121*, 10525. (b) Kishimoto, N.; Hagihara, Y.; Ohno, K.; Knippenberg, S.; François, J.-P.; Deleuze, M. S. *J. Phys. Chem. A* **2005**, *109*, 9324.

(15) (a) Brion, C. E.; Zheng, Y.; Rolke, J.; Neville, J. J.; McCarthy, I. E.; Wang, J. *J. Phys. B* **1998**, *31*, L223. (b) Ren, X. G.; Ning, C. G.; Deng, J. K.; Zhang, S. F.; Su, G. L.; Huang, F.; Li, G. Q. *Phys. Rev. Lett.* **2005**, *94*, 163201.

(16) Köppel, H.; Domcke, W.; Cederbaum, L. S. *Adv. Chem. Phys.* **1984**, *57*, 59.

(17) Heeger, A. J. In *Conjugated Polymers*; Salaneck, W. R., Lundström, I., Rånby, B., Eds.; Oxford University Press: New York, 1993.

(18) Kwiatkowski, J. S.; Leszczynski, J.; Teca, I. *J. Mol. Struct.* **1997**, *437*, 451.

(19) *Thiophene and Its Derivatives*; Weissberger, A., Taylor, C. E., Gronowitz, S., Eds.; The Chemistry of Heterocyclic Compounds, Vols. 3 and 44; Wiley-Interscience: New York, 1952/1992.

(20) Marseglia, E. A.; Grepioni, F.; Tedesco, E.; Braga, D. *Mol. Cryst. Liq. Cryst.* **2000**, *348*, 137.

(21) Barbarella, G.; Zambianchi, M.; Bongini, A.; Antolini, L. *Adv. Mater.* **1993**, *5*, 834.

(22) Horowitz, G. J. *Mater. Chem.* **1999**, *9*, 2021.

(23) Katz, H. E.; Bao, Z. *J. Phys. Chem. B* **2000**, *104*, 671.

(24) Kai, X.; Yun, Q. L.; Ting, Q.; Wei, Z. *J. Am. Chem. Soc.* **2005**, *127*, 13281.

(25) Kishimoto, N.; Yamakado, H.; Ohno, K. *J. Phys. Chem.* **1996**, *100*, 8204.

(26) Derrick, P. J.; Åsbrink, L.; Edqvist, O.; Jonsson, B.-Ö.; Lindholm, E. *Int. J. Mass Spectrom. Ion Phys.* **1971**, *6*, 177.

(27) Klasinc, L.; Sabljic, A.; Kluge, G.; Rieger, J.; Scholz, M. *J. Chem. Soc., Perkin Trans. 2* **1982**, *539*.

(28) Bawagan, A. D. O.; Olsson, B. J.; Tan, K. H.; Chen, J. M.; Yang, B. X. *Chem. Phys.* **1992**, *164*, 283.

(29) Holland, D. M. P.; Karlsson, L.; von Niessen, W. *J. Electron Spectrosc. Relat. Phenom.* **2001**, *113*, 221.

(30) Wang, H.; Feifel, R.; Miron, C.; Karlsson, L.; Svensson, S. *J. Chem. Phys.* **2002**, *117*, 7587.

(31) Chambers, S. A.; Tomas, T. D. *J. Chem. Phys.* **1977**, *67*, 2596.

(32) Giertz, A.; Bässler, M.; Björneholm, O.; Wang, H.; Feifel, R.; Miron, C.; Karlsson, L.; Svensson, S. *J. Chem. Phys.* **2000**, *117*, 7587.

(33) Munakata, T.; Kuchitsu, K. *J. Electron Spectrosc. Relat. Phenom.* **1980**, *20*, 235.

(34) Zhang, S. F.; Ren, X. G.; Su, G. L.; Ning, C. G.; Zhou, H.; Li, B.; Li, G. Q.; Deng, J. K. *Chem. Phys.* **2006**, *327*, 269.

(35) Ning, C. G.; Hajgató, B.; Huang, Y. R.; Zhang, S. F.; Liu, K.; Luo, Z. H.; Knippenberg, S.; Deng, J. K.; Deleuze, M. S. *Chem. Phys.* **2008**, *343*, 19.

(36) Deleuze, M. S.; Giuffreda, M. G.; François, J.-P.; Cederbaum, L. S. *J. Chem. Phys.* **1999**, *111*, 5851.

(37) Deleuze, M. S.; Cederbaum, L. S. *Adv. Quantum. Chem.* **1999**, *35*, 77.

(38) Deleuze, M. S.; Giuffreda, M. G.; François, J.-P.; Cederbaum, L. S. *J. Chem. Phys.* **2000**, *112*, 5325.

(39) Deleuze, M. S.; Giuffreda, M. G.; François, J.-P. *J. Phys. Chem. A* **2002**, *106*, 5626.

(40) Deleuze, M. S.; Trofimov, A. B.; Cederbaum, L. S. *J. Chem. Phys.* **2001**, *115*, 5859.

(41) Bieri, G.; Asbrink, L. and von Niessen, W. *J. Electron Spectrosc.* **1982**, *22*, 129.

(42) Cederbaum, L. S. and Domcke, W. *Adv. Chem. Phys.* **1977**, *36*, 205.

(43) Öhrn, Y.; Born, G. *Adv. Quantum Chem.* **1981**, *13*, 1.

(44) Ortiz, J. V. In *Computational Chemistry: Reviews of Current Trends*; J., Leszczynski, J., Ed.; World Scientific: Singapore, 1997; Vol. 2, p 1.

(45) von Niessen, W.; Schirmer, J.; Cederbaum, L. S. *Comput. Phys. Rep.* **1984**, *1*, 57.

(46) Schirmer, J.; Cederbaum, L. S.; Walter, O. *Phys. Rev. A* **1983**, *28*, 1237.

(47) Weikert, H.-G.; Meyer, H.-D.; Cederbaum, L. S.; Tarantelli, F. *J. Chem. Phys.* **1996**, *104*, 7122.

(48) Schirmer, J.; Angonoa, G. *J. Chem. Phys.* **1989**, *91*, 1754.

(49) Ehara, M.; Ohtsuka, Y.; Nakatsuji, H.; Takahashi, M.; Udagawa, Y. *J. Chem. Phys.* **2005**, *122*, 234319.

(50) Nakatsuji, H.; Kital, O.; Yonezawa, T. *J. Chem. Phys.* **1985**, *83*, 723.

(51) Trofimov, A. B.; Köppel, H.; Schirmer, J. *J. Chem. Phys.* **1998**, *109*, 1025.

(52) (a) Derrick, P. J.; Åsbrink, L.; Edqvist, O.; Lindholm, E. *Spectrochim. Acta A* **1971**, *27*, 2525. (b) Derrick, P. J.; Åsbrink, L.; Edqvist, O.; Jonsson, B.-Ö.; Lindholm, E. *Int. J. Mass Spectrom. Ion Phys.* **1971**, *6*, 191.

(53) Møller, C.; Plesset, M. S. *Phys. Rev.* **1934**, *46*, 618.

(54) (a) Cederbaum, L. S.; Domcke, W. *Adv. Chem. Phys.* **1977**, *36*, 205. (b) Zakrzewski, V. G.; von Niessen, W. *J. Comput. Chem.* **1993**, *14*, 13.

(55) Deleuze, M. S.; Cederbaum, L. S. *Int. J. Quantum Chem.* **1997**, *63*, 483.

(56) (a) Deleuze, M. S. *J. Chem. Phys.* **2002**, *116*, 7012. (b) Deleuze, M. S. *J. Phys. Chem. A* **2004**, *108*, 9244. (c) Deleuze, M. S. *Chem. Phys.* **2006**, *329*, 22.

(57) Potts, A. W.; Holland, D. M. P.; Trofimov, A. B.; Schirmer, J.; Karlsson, L.; Siegbahn, K. *J. Phys. B* **2003**, *36*, 3129.

(58) Potts, A. W.; Edvardson, D.; Karlsson, L.; Holland, D. M. P.; MacDonald, M. A.; Hayes, M. A.; Maripuu, R.; Siegbahn, K.; von Niessen, W. *Chem. Phys.* **2000**, *254*, 385.

(59) Trofimov, A. B.; Schirmer, J.; Holland, D. M. P.; Karlsson, L.; Maripuu, R.; Siegbahn, K.; Potts, A. W. *Chem. Phys.* **2001**, *263*, 167.

(60) Potts, A. W.; Trofimov, A. B.; Schirmer, J.; Holland, D. M. P.; Karlsson, L. *Chem. Phys.* **2001**, *271*, 337.

(61) Trofimov, A. B.; Schirmer, J.; Holland, D. M. P.; Potts, A. W.; Karlsson, L.; Maripuu, R.; Siegbahn, K. *J. Phys. B* **2002**, *35*, 5051.

(62) Ren, X. G.; Ning, C. G.; Deng, J. K.; Zhang, S. F.; Su, G. L.; Huang, F.; Li, G. Q. *Rev. Sci. Instrum.* **2005**, *76*, 063103.

(63) Ning, C. G.; Ren, X. G.; Deng, J. K.; Su, G. L.; Zhang, S. F.; Knippenberg, S.; Deleuze, M. S. *Chem. Phys. Lett.* **2006**, *421*, 52.

(64) Duffy, P.; Chong, D. P.; Casida, M. E.; Salahub, D. R. *Phys. Rev. A* **1994**, *50*, 4707.

(65) Davidson, E. R. *Can. J. Phys.* **1996**, *74*, 757.

(66) Feller, D. *J. Chem. Phys.* **1992**, *96*, 6104.

(67) Martin, J. M. L.; El-Yazal, J.; François, J.-P. *Mol. Phys.* **1995**, *86*, 1437. See also: Koch, W.; Holthausen, M. C. A. *A chemist's guide to density functional theory*, 2nd ed.; V. C. H. Wiley: Weinheim, Germany, 2001.

(68) Frisch, M. J.; *et mult. al. Gaussian 03*, revision D.01; Gaussian, Inc.: Wallingford, CT, 2004.

(69) Schmidt, M. W.; Baldridge, K. K.; Jensen, J. H.; Koseki, S.; Gordon, M. S.; Nguyen, K. A.; Windus, T. L.; Elbert, S. T. *QCPE Bull.* **1990**, *10*, 52.

(70) (a) Ruhe, A. *Math. Comput.* **1979**, *33*, 680. (b) Meyer, H.-D.; Pal, S. *J. Chem. Phys.* **1989**, *91*, 6195.

(71) (a) Liu, B. *Numerical Algorithms in Chemistry, Algebraic Methods, LBL-8158*; Lawrence Berkeley Laboratory: Berkeley, California. (b) Tarantelli, F.; Sgamellotti, A.; Cederbaum, L. S.; Schirmer, J. *J. Chem. Phys.* **1987**, *86*, 2201.

(72) Dunning, T. H., Jr. *J. Chem. Phys.* **1989**, *90*, 1007.

(73) See various contributions to the original HEMS program as recorded by Bawagan [A. O. Bawagan, Ph.D. Thesis, University of British Columbia (UBC), 1987]. The HEMS (now known as MOMAP) program has been extensively revised and extended at UBC by N. M. Cann and G. Cooper.

(74) (a) Mathar, R. J. *Int. J. Quantum Chem.* **2002**, *90*, 227. (b) Lentz, W. J. *Appl. Opt.* **1976**, *15*, 668.

(75) Duffy, P.; Casida, M. E.; Brion, C. E.; Chong, D. P. *Chem. Phys.* **1992**, *159*, 347.

(76) Köppel, H.; Domcke, W.; Cederbaum, L. S. *Adv. Chem. Phys.* **1984**, *57*, 59.

(77) Deleuze, M. S.; Denis, J.-P.; Delhalle, J.; Pickup, B. T. *J. Phys. Chem. A* **1993**, *97*, 5115.

(78) (a) Pickup, B. T.; Goscinski, O. *Mol. Phys.* **1973**, *26*, 1013. (b) Szabo, A.; Ostlund, N. S. In *Modern Quantum Chemistry*; McGraw-Hill, Inc.: New York, 1989; Chapter 7.

(79) Golod, A.; Deleuze, M. S.; Cederbaum, L. S. *J. Chem. Phys.* **1999**, *110*, 6014.

(80) (a) Takahashi, M.; Otsuka, K.; Udagawa,Y. *Chem. Phys.* **1998**, *227*, 375. (b) Takahashi, M.; Ogino, R.; Udagawa, Y. *Chem. Phys. Lett.* **1998**, *288*, 821.